Digital Comprehensive Summaries of Uppsala Dissertations
from the Faculty of Science and Technology 2516

Model-Based Design and Validation of Advanced Mechatronic Systems illustrated by Modern Steer-by-Wire Systems

MARCUS IRMER

ACTA UNIVERSITATIS
UPSALIENSIS
2025

ISSN 1651-6214
ISBN 978-91-513-2426-5
urn:nbn:se:uu:diva-552408

UPPSALA
UNIVERSITET

Dissertation presented at Uppsala University to be publicly examined in Lecure hall Eva von Bahr, Ångströmlaboratoriet, Lägerhyddsvägen 1, Uppsala, Monday, 12 May 2025 at 13:00 for the degree of Doctor of Philosophy. The examination will be conducted in English. Faculty examiner: PhD Matthijs Klomp (Volvo Car Corporation).

Abstract
Irmer, M. 2025. Model-Based Design and Validation of Advanced Mechatronic Systems illustrated by Modern Steer-by-Wire Systems. *Digital Comprehensive Summaries of Uppsala Dissertations from the Faculty of Science and Technology* 2516. 98 pp. Uppsala: Acta Universitatis Upsaliensis. ISBN 978-91-513-2426-5.

The automotive industry is experiencing a significant transformation driven by the demand for automation, autonomy and resource reduction. A key factor in this transformation is the model-based design and validation of advanced vehicle systems, particularly Steer-by-Wire systems, which are essential for highly automated and autonomous vehicles. However, Steer-by-Wire systems, characterized by the absence of a mechanical connection between the steering wheel and the front wheels, present unique challenges for achieving robust control as well as ensuring driving comfort and safety. This dissertation addresses these challenges by exploring innovative approaches for the optimal control of Steer-by-Wire systems, highlighting the model-based design and the integration of simulation environments. For this, a detailed model is developed, considering all relevant degrees of freedom and nonlinear characteristics of a real Steer-by-Wire system. Based on this detailed model, the dissertation presents a novel multivariable control approach that enhances the robustness and performance of Steer-by-Wire systems compared to traditional designs. The derived control approach demonstrates improved system stability and performance, effectively addressing parameter uncertainties and varying driving conditions. These satisfactory characteristics are validated both in an augmented simulation environment and on a real prototype. By combining virtual testing within the augmented simulation environment with real-world prototyping, the need for labor-intensive physical testing is minimized, thus optimizing development resources and time. The presented methods are not only employed for the development of Steer-by-Wire systems, but also for further applications in automotive engineering, including driver assistance systems, sensor evaluations and perception systems. In conclusion, the research contributes to mechatronics and automotive engineering by advancing autonomous driving through robust control approaches, virtual testing and agile development strategies. The insights and methodologies proposed not only advance the development of novel Steer-by-Wire systems, but can also serve as a basis for future innovations in mechatronic systems that require precise control and reliability.

Keywords: Mechatronic Systems, Vehicle Dynamics Systems, Steer-by-Wire Systems, Modeling, Optimal Control Theory, Robustness Analysis

Marcus Irmer, Department of Electrical Engineering, Electricity, Box 65, Uppsala University, SE-751 03 Uppsala, Sweden.

ISSN 1651-6214
ISBN 978-91-513-2426-5
URN urn:nbn:se:uu:diva-552408 (http://urn.kb.se/resolve?urn=urn:nbn:se:uu:diva-552408)

„Die Freiheit der Erwachsenen heißt Verantwortung“
– Joachim Gauck

List of Papers

This dissertation is based on the following papers, which are referred to in the text by their Roman numerals:

I. **Irmer, M.**, Degen, R., Nüßgen, A., Thomas, K., Henrichfreise, H., Ruschitzka, M., "Development and Analysis of a Detail Model for Steer-by-Wire Systems," *IEEE Access*, Vol. 11, pp. 7229-7236, January 2023.

II. **Irmer, M.**, Thomas, K., Ruschitzka, M., Henrichfreise, H., "Design of a Robust Optimal Multivariable Control for a Steer-by-Wire System," *SAE Technical Paper*, 2023-01-1218, June 2023.

III. **Irmer, M.**, Degen, R., Thomas, K., Ruschitzka, M., "Direct Discrete Design of a Multivariable LQG Compensator with Combined Discretization applied to a Steer-by-Wire System," *Proc. Automotive meets Electronics*, June 2023, Dortmund, Germany.

IV. **Irmer, M.**, Rosenthal, R., Nüßgen, A., Degen, R., Thomas, K., Ruschitzka, M., "Design of a Model-Based Optimal Multivariable Control for the Individual Wheel Slip of a Two-Track Vehicle," *SAE Technical Paper*, 2023-01-1219, June 2023.

V. **Irmer, M.**, Kalder, I., Tönnemann, M., Rüggeberg, L., Degen, R., Thomas, K., Ruschitzka, M., "Point Cloud based 3D Trafficability Analysis for Large-Volume and Heavy-Duty Transports," *submitted to IET Intelligent Transport Systems*, September 2024.

VI. **Irmer, M.**, Ott, H., Degen, R., Nüßgen, A., Thomas, K., Ruschitzka, M., "Methodical Data Collection for Light Electric Vehicles to validate Simulation Models and fit AI-based Driver Assistance Systems," *Proc. Kolloquium Future Mobility*, June 2022, Ostfildern, Germany.

VII. Degen, R., Tauber, A., **Irmer, M.**, Nüßgen, A., Klein, F., Schyr, C., Leijon, M., Ruschitzka, M., "Integration of Vulnerable Road Users Behavior into a Virtual Test Environment for Highly Automated Mobility Systems," *Proc. Kolloquium Future Mobility*, June 2022, Ostfildern, Germany.

VIII. Degen, R., Tauber, A., Nüßgen, A., **Irmer, M.**, Klein, F., Schyr, C., Leijon, M., Ruschitzka, M., "Methodical Approach to Integrate Human Movement Diversity in Real-Time into a Virtual Test Field for Highly Automated Vehicle Systems," *Journal of Transportation Technologies*, Vol. 12, No. 3, pp. 296-309, July 2022.

IX. Degen, R., Nüßgen, A., **Irmer, M.**, Klein, F., Schyr, C., Leijon, M., Ruschitzka, M., "Data Flow Management Requirements for Virtual Testing of Highly Automated Vehicles," *Proc. AVL German Simulation Conference*, September 2022, Regensburg, Germany.

X. Degen, R., de Fries, M., Nüßgen, A., **Irmer, M.**, Leijon, M., Ruschitzka, M., "Stereoscopic Camera-Sensor Model for the Development of Highly Automated Driving Functions within a Virtual Test Environment," *Journal of Transportation Technologies*, Vol. 13, No. 1, pp. 87-114, January 2023.

XI. Nüßgen, A., Degen, R., **Irmer, M.**, Boström, C., Ruschitzka, M., "Intelligent Analysis of Components with Regard to Significant Features for Subsequent Classification," *SAE Technical Paper*, 2023-01-1213, June 2023.

XII. Nüßgen, A., Richter, F., Krach, N., **Irmer, M.**, Degen, R., Boström, C., Ruschitzka, M., "Robustness and Sensitivity of Artificial Neural Networks for Mechatronic Product Development," *Proc. Automotive meets Electronics*, June 2023, Dortmund, Germany.

XIII. Nüßgen, A., Degen, R., **Irmer, M.**, Richter, F., Boström, C., Ruschitzka, M., "Leveraging Robust Artificial Intelligence for Mechatronic Product Development – A Literature Review," *International Journal of Intelligence Science*, Vol. 14, pp. 1-21, January 2024.

XIV. de Fries, M., **Irmer, M.**, Thomas, K., Degen, R., "Innovative Test Field Approach for Agricultural Applications," *Proc. Fachtagung TestRig*, September 2024, Ostfildern, Germany.

XV. Nüßgen, A., Lerch, A., Degen, R., **Irmer, M.**, de Fries, M., Richter, F., Boström, C., Ruschitzka, M. "Reinforcement Learning in Mechatronic Systems: A Case Study on DC Motor Control," *Circuits and Systems*, Vol. 16, No. 1, pp. 1-24, January 2025.

Reprints were made with permission from the respective publishers.

Other contributions of the author, not included in this dissertation:

XVI. **Irmer, M**., "Detailed Model-Based Design and Validation of a Highly Robust LQG Control of the Driver's Steering Torque for a Steer-by-Wire System and Development of a Methodology for the Objectification of Steering Feel," *Proc. Akademietag Nürburgring Akademie*, November 2022, Nürburgring, Germany.

XVII. Nüßgen, A., Richter, F., Degen, R., **Irmer, M.**, Boström, C., Ruschitzka, M., "Intelligent Component Manufacturability Testing in Virtual Product Development," *Proc.* NAFEMS Artificial Intelligence und Machine Learning in der CAE-basierten Simulation, October 2023, Munich, Germany.

XVIII. Ruschitzka, M., de Fries, M., **Irmer, M.**, Nüßgen, A., "KI in der Entwicklung & Produktion – Ein Schritt-für-Schritt-Leitfaden zur Programmierung Künstlicher Intelligenz," *Trend-Auto2030plus Guide*, September 2024.

XIX. Röttgermann, S., Albrecht, D., de Fries, M., **Irmer, M.**, "Methodical Approach and Analysis of Highly Realistic Virtual Worlds as a Test Environment for the Evaluation of Disturbance Detection and Work Quality Monitoring Algorithms in the Agricultural Domain," *Proc. IFToMM Young Faculty Group Symposium on Emerging Fields in Mechanism and Machine Science*, November 2024, Duisburg, Germany.

XX. de Fries, M., **Irmer, M.**, Röttgermann, S., Thomas, K., Degen, R., “Methodical Approach on precise Reproduction of real Images by Camera Modelling in highly realistic Virtual Test Environments,” *submitted to Results in Engineering*, January 2025.

Contents

Abbreviations

The capitalization of the following words is intended to indicate the notation of the abbreviations.

aff	afference
AU	Axle Unit
c	control
CNS	Central Nervous System
CoG	Center of Gravity
d	disturbance
DA	Driver Actuation
eMF	extrafusal Muscle Fiber
EPS	Electromechanical Power Steering
FU	Feedback Unit
HMI	Human-Machine Interface
iMF	intrafusal Muscle Fiber
LQE	Linear-Quadratic Estimator
LQG	Linear-Quadratic-Gaussian
LQR	Linear-Quadratic Regulator
m	measurement
M	Muscle
MA	Axle Motor
MDC	Mechatronic Development Cycle
MF	Feedback Motor
o	objective
p	plant
$\tilde{p}$	reduced plant
r	reference
R	Rack
rq	requested
S	Steering wheel
SbW	Steer-by-Wire
SC	Steering angle Control loop
SISO	Single-Input Single-Output

TB	Torsion Bar
V	Vehicle
VD	Vehicle Dynamics
WFL	Left Front Wheel
WFR	Right Front Wheel
WL	Left front Wheel
WR	Right front Wheel
WRL	Left Rear Wheel
WRR	Right Rear Wheel
zoh	zero-order-hold

Nomenclature

a_{aff}	factor for calculation of the afferences
$\underline{A}_D$	system matrix of the discrete augmented plant model for the LQR resp. LQE design
$\underline{A}_p$	system matrix of the plant model
$\underline{A}_{\tilde{p}}$	system matrix of the reduced plant model
$\underline{A}_{SC}$	system matrix of the model for the steering angle control loop
$\underline{B}_{cD}$	control input matrix of the discrete augmented plant model for the LQE design
$\underline{B}_D$	input matrix of the discrete augmented plant model for the LQR resp. LQE design
b_{DA}	viscous damping constant of the reduced DA model
b_e	viscous damping constant of the eMF
b_i	viscous damping constant of the iMF
$\underline{B}_{pc}$	control input matrix of the plant model
$\underline{B}_{\tilde{p}c}$	control input matrix of the reduced plant model
$\underline{B}_{pd}$	disturbance input matrix of the plant model
$\underline{B}_{\tilde{p}d}$	disturbance input matrix of the reduced plant model
b_S	viscous friction of the steering wheel
$\underline{B}_{SC}$	input matrix of the model for the steering angle control loop
$\underline{C}_D$	output matrix of the discrete augmented plant model for the LQR resp. LQE design
c_{DA}	stiffness of the reduced DA model
c_{ep}	stiffness of the parallel spring of the eMF
c_{es}	stiffness of the serial spring of the eMF
c_{ip}	stiffness of the parallel spring of the iMF
c_{is}	stiffness of the serial spring of the iMF
$\underline{C}_{po}$	objective output matrix of the plant model
$\underline{C}_{\tilde{p}o}$	objective output matrix of the reduced plant model
$\underline{C}_{SC}$	output matrix of the model for the steering angle control loop
c_{TB}	stiffness of the torsion bar
$\underline{D}_{cD}$	control feedthrough matrix of the discrete augmented plant model for the LQE design

$\underline{D}_D$	feedthrough matrix of the discrete augmented plant model for the LQR resp. LQE design
$\underline{D}_{SC}$	feedthrough matrix of the model for the steering angle control loop
e_{sR}	control error of the deflection of the rack
e_{TTB}	control error of the torsion bar torque
F_{ces}	spring force of the serial spring of the eMF
F_{cis}	spring force of the serial spring of the iMF
F_{cns}	actuating force of the CNS
$\underline{F}_D$	noise filter matrix of the discrete augmented plant model for the LQE design
F_e	actuating force of the eMF
F_i	actuating force of the iMF
F_R	rack force
F_{reflex}	reflex force
F_S	muscle force
J_{MF}	moment of inertia of the FU motor
J_S	moment of inertia of the steering wheel
k	index for characterizing the point in time
$\underline{K}$	optimal LQR gain matrix
$\underline{\hat{K}}$	optimal LQE gain matrix
K_{Ia}	factor for calculation of the reflex force
n	number of state variables of the discrete augmented plant model for the LQR resp. LQE design
n_p	number of state variables of the plant model
p	number of input variables of the discrete augmented plant model for the LQR resp. LQE design
$\underline{\tilde{P}}$	stationary covariance matrix of the a-priori estimation error
p_c	number of control input variables of the plant model
p_d	number of disturbance input variables of the plant model
q	number of output variables of the discrete augmented plant model for the LQR resp. LQE design
$\underline{Q}$	positive semidefinite weighting matrix for the LQR design to penalize the control errors
q_m	number of measurement output variables of the plant model
q_o	number of objective output variables of the plant model
$\underline{R}$	positive definite weighting matrix for the LQR design to penalize the use of the control variables
r_S	steering wheel radius

$\underline{S}$	matrix representing the positive definite solution of the algebraic matrix Riccati equation for the LQR design
S_{Ia}	sensor signal of the position error of the muscle deflection
S_{II}	sensor signal of the approximated muscle deflection
s_M	deflection of the muscle
s_{Mrq}	requested deflection of the muscle
s_R	deflection of the rack
s_{Rrq}	requested deflection of the rack
s_{Vx}	translational degree of freedom in x-direction of the vehicle
s_{Vy}	translational degree of freedom in y-direction of the vehicle
t	time
T	sample time
T_D	drive torque of the vehicle
T_{MA}	AU motor torque
T_{MArq}	requested AU motor torque
T_{MF}	FU motor torque
T_{MFrq}	requested FU motor torque
T_S	steering torque
T_{TB}	torsion bar torque
T_{TBrq}	requested torsion bar torque
T_{WL}	torque about the steering axis of the left front wheel
T_{WR}	torque about the steering axis of the right front wheel
$\underline{u}$	input vector of the augmented plant model for the LQR design
$\underline{u}_d$	input vector of the disturbance model for the LQE design
$\underline{u}_{d,k}$	input vector of the discrete disturbance model for the LQE design
$u_{DAr,k}$	reference input variable of the discrete DA model
$\underline{u}_k$	input vector of the discrete augmented plant model for the LQR resp. LQE design
$\underline{u}_{pc}$	control input vector of the plant model
$\underline{u}_{pc,k}$	control input vector of the discrete plant model
$\underline{u}_{pd}$	disturbance input vector of the plant model
$\underline{u}_{pd,k}$	disturbance input vector of the discrete plant model
$\underline{u}_{SC}$	input vector of the model for the steering angle control loop
$\underline{u}_{VDr,k}$	reference input vector of the discrete VD model
$\underline{u}_{wp}$	plant input vector of the weighting model for the LQR design
$\underline{u}_{wr}$	reference input vector of the weighting model for the LQR design
$\underline{V}$	positive semidefinite intensity matrix of the process noise

$\underline{v}_d$	vector of process noise for the disturbance model for the LQE design
$\underline{v}_{d,k}$	vector of process noise for the discrete disturbance model for the LQE design
$\underline{v}_k$	vector of process noise of the discrete augmented plant model for the LQE design
v_M	deflection velocity of the muscle
v_{Mrq}	requested deflection velocity of the muscle
$\underline{v}_{pc}$	vector of process noise for the plant model
$\underline{v}_{pc,k}$	vector of process noise for the discrete plant model
v_V	translational vehicle velocity
$\underline{w}$	vector of measurement noise for the plant model
$\underline{W}$	positive definite intensity matrix of the measurement noise
$\underline{w}_k$	vector of measurement noise for the discrete plant model
$\underline{x}_0$	initial state vector of the discrete augmented plant model for the LQR resp. LQE design
$\tilde{\underline{x}}_0$	initial a-priori estimate of the state vector of the discrete augmented plant model for the LQE design
$\underline{x}_{d,0}$	initial state vector of the disturbance model for the LQR design
$\underline{x}_{d,k}$	state vector of the discrete disturbance model for the LQE design
$\tilde{\underline{x}}_{d,k}$	a-priori estimate of the disturbance variables of the discrete plant model
$\hat{\underline{x}}_{d,k}$	a-posteriori estimate of the disturbance variables of the discrete plant model
x_{DA}	state variable of the reduced DA model
$\underline{x}_k$	state vector of the discrete augmented plant model for the LQR resp. LQE design
$\tilde{\underline{x}}_k$	a-priori estimate of the state vector of the discrete augmented plant model for the LQE design
$\hat{\underline{x}}_k$	a-posteriori estimate of the state vector of the discrete augmented plant model for the LQE design
$\underline{x}_p$	state vector of the plant model
$\underline{x}_{\tilde{p}}$	state vector of the reduced plant model
$\underline{x}_{p,0}$	initial state vector of the plant model
$\underline{x}_{\tilde{p},0}$	initial state vector of the reduced plant model
$\underline{x}_{p,k}$	state vector of the discrete plant model
$\tilde{\underline{x}}_{p,k}$	a-priori estimate of the state variables of the discrete plant model

$\underline{\hat{x}}_{p,k}$	a-posteriori estimate of the state variables of the discrete plant model
$\underline{x}_{r,k}$	reference vector of the discrete LQG compensator
$\underline{x}_{SC}$	state vector of the model for the steering angle control loop
$\underline{x}_{SC,0}$	initial state vector of the model for the steering angle control loop
$\underline{y}$	output vector of the augmented plant model for the LQR resp. LQE design
$\underline{y}_d$	output vector of the disturbance model for the LQR resp. LQE design
$y_{DAp,k}$	plant output variable of the discrete DA model
$\underline{y}_k$	output vector of the discrete augmented plant model for the LQR resp. LQE design
$\underline{\tilde{y}}_k$	estimate of the noisy measurement output vector of the discrete plant model
$\underline{y}_{pm}$	measurement output vector of the plant model
$\underline{y}_{pm,k}$	measurement output vector of the discrete plant model
$\underline{y}_{po}$	objective output vector of the plant model
$\underline{y}_{po,k}$	objective output vector of the discrete plant model
$\underline{y}_r$	output vector of the reference model for the LQR design
$\underline{y}_{SC}$	output vector of the model for the steering angle control loop
$\underline{y}_{VDm,k}$	measurement output vector of the discrete VD model
$y_{VDp,k}$	plant output variable of the discrete VD model
$\underline{y}_w$	output vector of the weighting model for the LQR design
β_V	side slip angle of the vehicle
θ_{WFL}	rotational degree of freedom of the left front wheel
θ_{WFR}	rotational degree of freedom of the right front wheel
θ_{WRL}	rotational degree of freedom of the left rear wheel
θ_{WRR}	rotational degree of freedom of the right rear wheel
$\underline{\mu}$	vector of friction coefficients between the tires of the vehicle and the road
φ_{MA}	AU motor angle
φ_{MArq}	requested AU motor angle
φ_S	steering wheel angle
φ_{Srq}	requested steering wheel angle
φ_{WL}	steering angle of the left front wheel
φ_{WR}	steering angle of the right front wheel
τ_{DA}	time constant of the reduced DA model
ψ_V	yaw angle of the vehicle
Ω_S	angular velocity of the steering wheel

Ω_{Srq}	requested angular velocity of the steering wheel
Ω_{WL}	angular velocity of the left front wheel
Ω_{WR}	angular velocity of the right front wheel

1 Introduction

The following chapter is adapted from the author's licentiate thesis [1].

This dissertation provides a comprehensive summary of the appended papers, which are the results of the author's research in the domain of model-based design of advanced vehicle control systems, virtual test environments and the application of artificial intelligence in mechatronic systems. The corresponding concepts are exemplified by Steer-by-Wire (SbW) systems.

In this chapter, the motivation for the research is explained. Based on this, the research questions are derived. Furthermore, an outline of the dissertation is presented.

1.1 Motivation and Research Questions

The future of transportation is expected to be dominated by highly automated and autonomous driving systems, with SbW as a key technology that offers several advantages: It can be dynamically adapted to different driving situations and thus increases driving comfort and agility. SbW also makes new steering modes possible: In highly automated driving, for instance, the steering wheel can move automatically without the driver physically interacting with it. In autonomous driving, SbW also makes it possible that the steering wheel no longer has to move at all. In this context, robust steering control is a fundamental requirement for automated vehicle lateral control. [2]-[4] However, current designs for steering controls often do not adequately address corresponding challenges such as dominant degrees of freedom, signal delays and nonlinear characteristics of the steering system [1]. Therefore, the objective of this dissertation is to develop and validate novel approaches for SbW systems and associated functions to improve their quality significantly. So, the following primary research question is addressed within this dissertation:

How can highly dynamic control approaches for modern SbW systems be designed, which simultaneously guarantee an extremely high robustness?

This main question leads to three more specific research questions:

1. How is a minimal and **optimal level of detail for modeling** the characteristics of a SbW system achievable?
2. How can a corresponding control algorithm for SbW systems already be **comprehensively virtually tested** in simulation under realistic conditions?
3. How can experiments that are currently being carried out with test vehicles be migrated to a **test bench** in order to obtain an **optimal prototype** at an early stage of development?

Fundamental for answering these questions is the approach of model-based design of mechatronic systems. Here, the focus is on optimal SbW models, which form the basis for all development steps, resulting in the structural design of the research according to Figure 1.1.

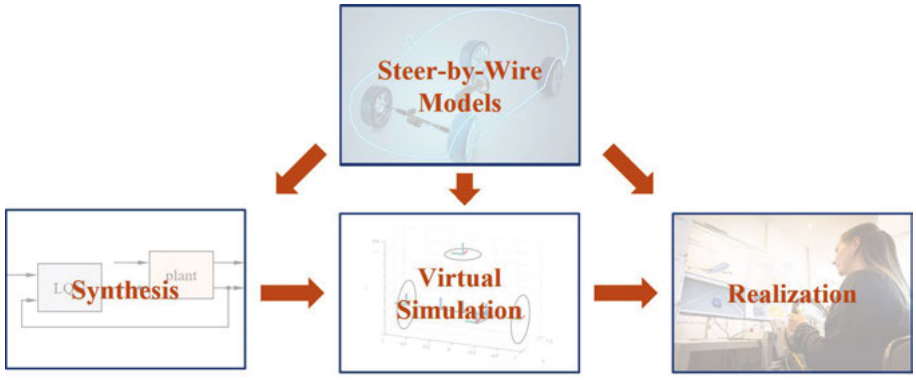

Figure 1.1 Structural design of the research.

The individual development steps are explained in the following chapters.

1.2 Outline of the Dissertation

The outline of the dissertation is derived from the structural design from Figure 1.1 and follows the mechatronic development circle (MDC) from Figure 1.2. The MDC is a development process for the prototype development of technical (mechatronic) systems with mechanical, electrical and information-processing components. Its aim is a prototype that exhibits optimal behavior according to the predefined requirements and objectives. For this, suitable models are essential. Hence, a novel detailed model of a SbW system is developed in step 1. In step 2, the dominant behavior of the SbW system is identified. Based on this, reduced optimal models of a SbW system are derived to

answer the first research question. These innovative models enable optimal results in every development step. Subsequent to the steps of modeling and model analysis, the model-based synthesis of a new control algorithm is performed in step 3. This control algorithm significantly enhances the robustness of the associated control system. The outstanding characteristics of the control algorithm are then validated through simulation in step 4 to answer the second research question. The result of this step is a validated control algorithm whose characteristics are satisfactory and guaranteed by mathematical methods, making extensive, costly and time-intensive testing on prototype vehicles redundant. Step 1 to step 4 are described in detail in the author's licentiate thesis [1]. This dissertation summarizes the main results of these steps.

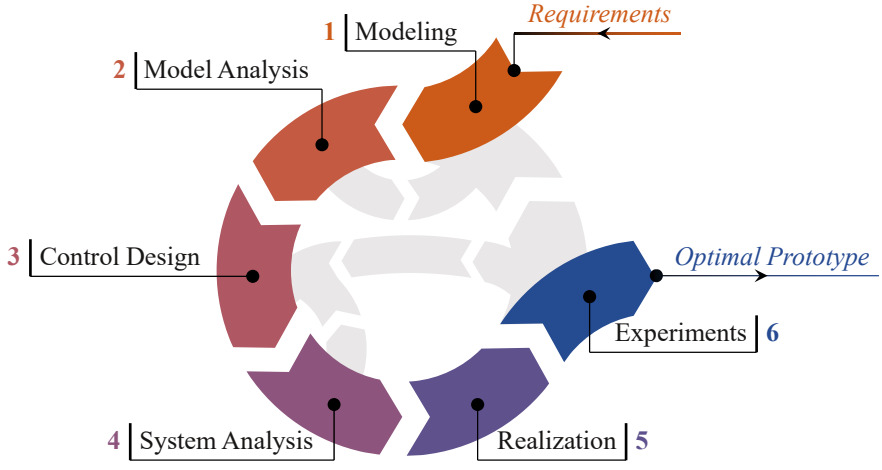

Figure 1.2. Mechatronic development cycle.

In addition, this dissertation addresses step 5 and step 6 of the MDC. In step 5, a test bench is realized in order to validate the control algorithm in a real-world environment, as described in step 6. Ideally, step 6 represents the final step of the MDC. Here, the same experiments are performed on the test bench as in the simulation (see step 4). If the measured results approximate the results from the simulation well enough, the MDC is exited with an optimal prototype and the third research question is answered in an optimal way.

The MDC is also represented in the structure of this dissertation. After a theoretical background on the research topic is given in Chapter 2 (*adapted from [1]*), Chapter 3 (*adapted from [1], Paper I*) describes the modeling and analysis of the developed detailed model of a SbW system. Chapter 4 (*enhanced from [1], Paper II, Paper III, Paper IV*) then presents the novel con-

trol design for the SbW system. The resulting controlled SbW system is analyzed in the simulation in Chapter 5 (*enhanced from [1], Paper II, Paper III, Paper IV, Paper V*). Chapter 6 (*new, Paper VI*) describes the realization of the control for the SbW system and reviews exemplary results of the subsequent experimental study. Afterwards, Chapter 7 (*enhanced from [1]*) provides a summary and conclusion.

Chapter 8 discusses potential future research, followed by a brief summary of each paper included in this dissertation in Chapter 9. Finally, a Swedish and German summary of the dissertation are presented in Chapter 10 and Chapter 11.

2 Theoretical Background

The following chapter is adapted from the author's licentiate thesis [1].

The objective of this chapter is to familiarize the reader with general definitions and methods for the development of mechatronic systems. First, an overview of the structure of a mechatronic system is given. Subsequently, the approaches of model-based design and virtual testing are presented. After that, an introduction to steering systems is given as one example of a complex mechatronic system, before the presented development process is applied to modern steering systems in form of SbW systems in the next chapter.

2.1 Definition of Mechatronic Systems

Mechatronic systems are integrated technical systems consisting of a mechanism, actuators (including power electronics and other electronics), sensors (including electronics for signal amplification and processing) and a control unit. The general structure of a mechatronic system is shown in Figure 2.1. This structure is a simplification that highlights the essential components and connections.

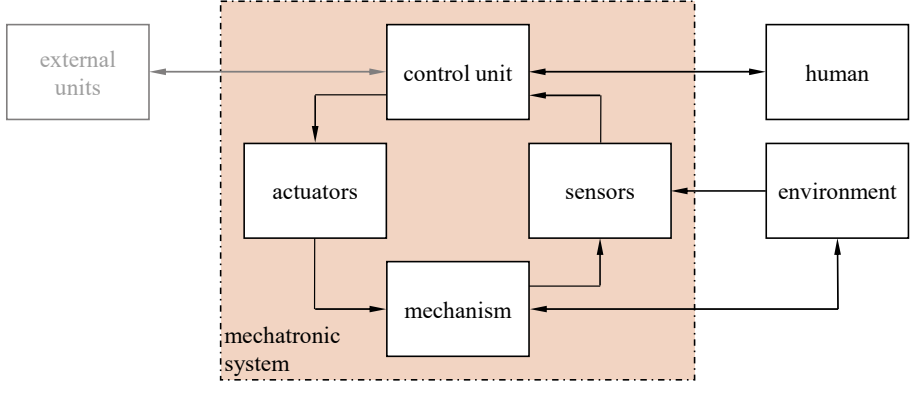

Figure 2.1. Structure of a mechatronic system.

In a mechatronic system, sensors are used to perceive the state of the mechanism and its environment. The sensor signals are processed by the control unit, which then generates signals to control the actuators. These actuators adjust the mechanism, changing its state towards the desired state. The sensors detect this change and forward the information back to the control unit. This interconnection of sensors, control unit, actuators and mechanism characterizes mechatronic systems as closed-loop systems. [5] In addition, mechatronic systems can interact with humans via a human-machine interface (HMI) and with other external units, as depicted in Figure 2.1. This interaction and the connection of the components through material, energy and information flow is indicated by arrows in this figure.

There are various process models for the development of a mechatronic system. One of the most common process models is the V-model [6]. It represents a continuous process from the requirements to a validated optimal mechatronic system. The structure of the simplified V-model is shown in Figure 2.2. The primary objective of the V-model is to assist in the development of mechatronic systems in which a mechanism, actuators and sensors should interact optimally through intelligent control units. To achieve this, the underlying development methodology leverages the expertise of mechanical engineering, electrical engineering, computer science, control engineering and simulation technology.

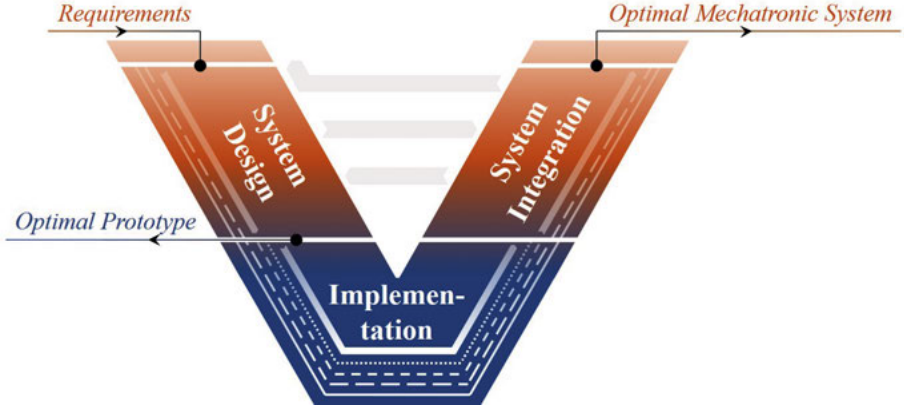

Figure 2.2. Structure of the simplified V-model.

The V-model is divided into three phases: system design, implementation and system integration. During system design, the requirements for the mechatronic system are first defined. Afterwards, the mechatronic system is designed as a prototype following the MDC, illustrated in Figure 1.2. The result

is an optimal prototype that fulfills the functional requirements. With the optimal prototype as the outcome of the system design, further development towards series production begins. This is the subject of the subsequent phase of implementation, where the domain-specific design of the individual components of the mechatronic system takes place. The individual components as well as the overall system are then tested and integrated in the third phase of system integration. The final result is an optimal mechatronic system that not only fulfills the functional requirements, but also additional requirements such as the cost-effective and simple production of the mechatronic system. More information regarding the V-model can be found in [6].

This dissertation concentrates on the phase of system design and the MDC within this phase applied to modern SbW systems.

2.2 Model-Based Design of Mechatronic Systems

Model-based design is a systematic approach for developing mechatronic systems, utilizing models as the central element throughout the entire development process. This approach enables the simulation, analysis and optimization of mechatronic systems before physical prototypes are built, thus reducing development time and costs while improving system performance and reliability. The approach of model-based design is deeply embedded in the MDC, as depicted in step 1 of Figure 1.2, and consequently also in the structural design of the author's research, illustrated in Figure 1.1.

The core concept of model-based design is to create mathematical models that represent the dominant behavior of the real mechatronic system. These models function as virtual prototypes that enable the evaluation of the system behavior and validation of suitable control approaches in early development stages. The models are constructed using standardized languages and frameworks such as CAE tools like MATLAB/Simulink [7].

The architecture for the model-based design and virtual testing follows the described structure of a mechatronic system consisting of several components. Mostly, the control unit of the mechatronic system is the central product whose development process should be supported by methods of model-based design. To enable the integrated development and testing of the control unit, it is advantageous to embed it in a modular environment consisting of models for the other components of the mechatronic system. Figure 2.3 illustrates an architecture for such a modular framework. The displayed architecture focuses on the essential components and connections. It emerges from the structure of a mechatronic system from Figure 2.1 by substituting its components with models. In general, the human is not included in the simulation environment.

However, if humans are part of the operating environment of the mechatronic system, their behavior and interaction with the mechatronic system can also be modeled in the environment model.

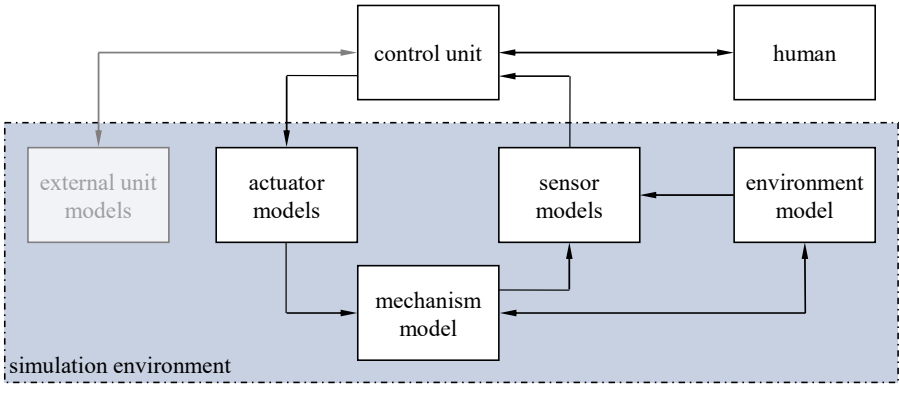

Figure 2.3. Architecture for model-based design and virtual testing.

The model-based design approach has several advantages regarding the development of mechatronic systems. It significantly enhances efficiency and cost-effectiveness by identifying potential issues early in the design phase. Additionally, the inherent flexibility of the models facilitates continuous improvement, enabling engineers to quickly iterate on designs in the simulation, incorporate new insights and adapt to evolving requirements or technological advances. Moreover, the models allow for virtual testing for comprehensive risk mitigation by evaluating system performance under extreme conditions and edge cases, which minimizes the likelihood of costly failures during physical testing and subsequent real-world applications. This approach of virtual testing is described in the next section.

2.3 Virtual Testing of Mechatronic Systems

Virtual environments offer a controlled setting in which various parameters of a mechatronic system can be manipulated to evaluate its performance under a wide range of conditions. This significantly accelerates the development process and enhances the robustness of the final system. Moreover, verification techniques, including Model-in-the-Loop, Software-in-the-Loop and Hardware-in-the-Loop, ensure a precise representation of the intended system behavior. Another critical aspect is the integration of control systems, so that corresponding control algorithms can be developed and tested within the vir-

tual environment, providing valuable insights into system stability and responsiveness. This integration facilitates a seamless transition from design to deployment by utilizing the same models for code generation. [8]

2.4 Lateral Control of a Vehicle

In the subsequent chapters, the approaches of model-based design and virtual testing are applied for the development of modern steering systems, which are employed for the lateral control of a vehicle. Therefore, a brief introduction to lateral control is given in the following section.

Driving a vehicle can be divided into two primary tasks: controlling the longitudinal and lateral motion of the vehicle. Longitudinal motion is controlled by the driver via the throttle and brake pedal. In contrast, lateral motion, encompassing translation in lateral direction and rotation around the vertical axis, is controlled by the driver using the steering wheel and the steering system. [9] Figure 2.4 presents a simplified block diagram of the resulting lateral control of a vehicle. In this context, the driver functions as the controller while the vehicle serves as the plant.

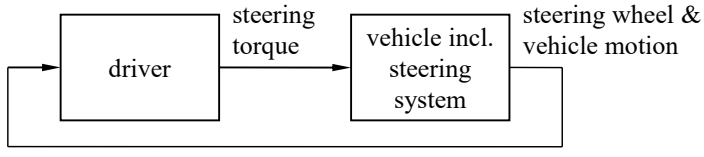

Figure 2.4. Simplified block diagram of the lateral control of a vehicle.

The driver perceives the lateral motion of the vehicle visually and kinesthetically. If this perceived motion deviates from the desired motion, the driver applies a torque at the steering wheel to adjust the lateral motion of the vehicle by deflecting the steering wheel and, consequently, the front wheels of the vehicle. This correction is perceived by the driver, resulting in a closed-loop system. The steering system represents the actuator in this closed-loop system. A robust steering system, which will be developed in the following chapters, is therefore essential to ensure safe lateral control of a vehicle. [1]

For more information on lateral control of vehicles as well as chassis and driving dynamics, refer to [10]-[12].

2.5 Function and Importance of Steering Systems

A steering system enables a driver of a vehicle to control the lateral motion of the vehicle. Its primary function is to convert the angle of the steering wheel into an angle of the front wheels of the vehicle. Additionally, the steering system must provide the driver with information regarding the current driving situation by giving appropriate feedback via the steering wheel [13]-[15]. This feedback sensed by the driver is called steering feel. The steering feel is a major factor in the overall driving experience [16]. Consequently, a large number of requirements are specified for the steering feel and the steering system [17]:

- Adequate steering torque and required steering wheel angle for the respective driving situation (steering power assistance up to 80 %)
- Good handling, reliability, sensitivity, accuracy and directness (e.g. precise steering without delay)
- Feedback on the condition of the contact between tire and road (e.g. friction coefficient)
- Automatic return to center position, good center feel and stabilizing behavior during all driving situations (e.g. no overshoot)
- Disturbance rejection and sufficient damping (e.g. shock suppression)
- Fulfillment of crash requirements
- Low energy consumption, noise, vibration, wear and maintenance

The evaluation of these individual requirements is highly subjective. In addition, many requirements are inherently in conflict with each other. These circumstances complicate the development of new steering systems. [1]

Since the steering system is crucial for the safety and control of a vehicle, developing robust steering systems is fundamental for the future realization of highly automated and autonomous driving technologies.

2.6 Definition of Steering Feel

Steering feel is the subjective experience of a driver of a vehicle based on the dynamic interaction between the driver and the vehicle. It encompasses the driver's visual, kinesthetic and haptic perceptions during steering. [16][18][19] The predominant component influencing the steering feel is the torque T_S that the driver induces resp. perceives at the steering wheel via the hands. This torque T_S is called steering torque. Hence, a desired steering feel directly results in a corresponding steering torque T_S. The two terms steering feel and steering torque are consequently closely connected.

In modern steering systems, the characteristics of the steering torque T_S can be designed almost arbitrarily. However, certain requirements must be fulfilled. For example, the steering torque T_S should provide the driver with essential feedback on relevant information regarding the road surface, such as variations in the friction coefficients between the tires of the vehicle and the road, as well as the driving situation, including phenomena like understeer or oversteer. Conversely, disturbance information, such as steering unsteadiness, bumps and vibrations, should ideally not be perceived by the driver. [20]

The tires are the only connection between the vehicle and the road. They transmit the forces and torques that lead to the longitudinal and lateral motion of the vehicle. During driving, the point of application of these forces and torques is shifted by the dynamic tire offset. This shift induces torques T_{WL} and T_{WR} about the steering axis of the left and right front wheel due to the lateral forces at the tires. These torques T_{WL} and T_{WR} are a nonlinear function of the current driving situation, the condition of the road and the contact between the tire and the road. [21] In conventional rack-and-pinion steering systems, the torques T_{WL} and T_{WR} about the steering axis of the left and right front wheel can be aggregated and transformed into an equivalent force F_R at the rack. This rack force F_R is proportional to the steering torque T_S experienced by the driver at the steering wheel, thereby providing feedback to the driver on the road surface and the current driving situation. [20] The rack force F_R is utilized for feedback because the torques T_{WL} and T_{WR} about the steering axis of the left and right front wheel cannot be estimated individually with the given measured variables. However, disturbances may persist in the rack force F_R. To ensure comfortable steering while suppressing the disturbances, only a part of the rack force F_R should be transmitted to the driver. The remainder has to be compensated by the steering control. Hence, the challenge is to design a reference generator for the steering feel and a corresponding control of the driver's steering torque which are capable of transmitting useful information at an adequate level while simultaneously suppressing disturbances. [1][22][23]

The reference generator for the steering feel is called feeling generator. An exemplary structure of a feeling generator is detailed in [24]. The approach for controlling the driver's steering torque is based on [25].

3 Development of a Model for Steer-by-Wire Systems

The following chapter is adapted from the author's licentiate thesis [1].

SbW systems have become a key technology for the deployment of highly automated and autonomous driving functions. Hence, they will be increasingly integrated into modern vehicles. The advantages of SbW systems are presented in Chapter 1.1 and [4][16][17]. The fundamental difference to conventional electromechanical power steering (EPS) systems, which are currently used, is that SbW systems no longer have a mechanical connection between the steering wheel and the front wheels. For more information on EPS systems, refer to [1][17]. This absence of mechanical redundancy in SbW systems poses a potential risk, as a malfunction in the steering control of the SbW system would make it impossible to control the lateral motion of a vehicle. This could lead to potentially dangerous situations. Consequently, ensuring high robustness of the steering control in any driving situation is essential for SbW systems [26][27]. However, current single-input single-output (SISO) control approaches cannot always guarantee such a high level of robustness. These approaches often show only limited robustness to degrees of freedom and nonlinear characteristics of the plant that are neglected in the control design [1]. In addition, the lack of a mechanical connection between the steering wheel and the front wheels makes it much more challenging to reproduce a realistic steering feel. An overview of the state of the art in the development of steering systems is given in [1][28]-[43].

To resolve the current issues, the subsequent chapters outline the methodical approach for the development of SbW systems which guarantees a high robustness of the resulting control system. To achieve this, a detailed model of a SbW system is developed that considers all relevant degrees of freedom and nonlinear characteristics that may occur in a real SbW system. This detailed model provides an accurate representation of an actual SbW system, qualifying it as a reliable plant model. The detailed plant model is presented in Chapter 3.1. The analysis of the detailed model is afterwards described in Chapter 3.2.

3.1 Modeling of a Steer-by-Wire System

This chapter describes the development of an innovative nonlinear detailed model of a SbW system as the first step of the MDC. The objective of this step is to develop a mathematical representation of a SbW system by transforming the different phenomena – mechanical, electrical, algorithmic and others – of the SbW system into a uniform representation based on equations. As an example, the individual process steps from the requirements to the model equations are depicted for the mechanical components in Figure 3.1, based on the Newton-Euler method described in [44]-[46].

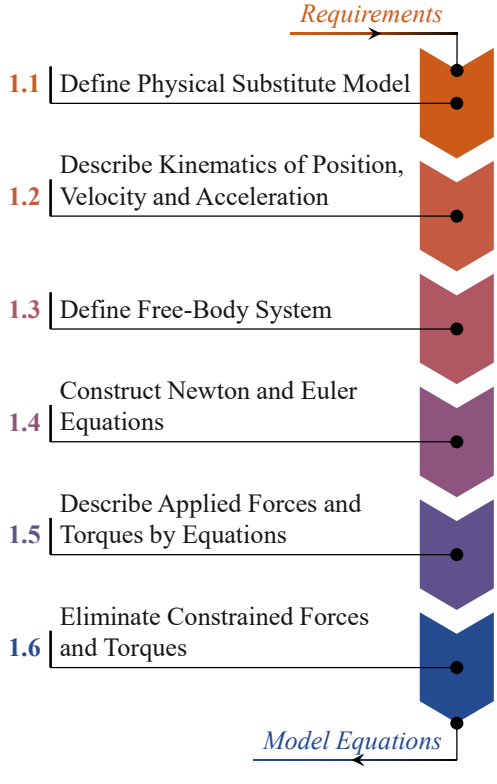

Figure 3.1. Process steps of the modeling.

The corresponding developed physical substitute model of the SbW system with nine degrees of freedom is illustrated in Figure 3.2. This model contains all relevant characteristics of a real SbW system. In Figure 3.2, the bodies of the physical substitute model are depicted in black, viscoelastic elements in red and gear ratios in gray. The resulting detailed SbW model can be divided into a submodel for the feedback unit (FU) and a submodel for the axle unit (AU). Both units are mechanically decoupled, illustrated by the green dashed

line in Figure 3.2. The FU model includes the steering wheel and a feedback actuator, which are connected to each other via a torsion bar [47]. The AU model, on the other hand, contains the front axle actuator, which is connected via a belt drive to a nut, which is further connected via a ball screw drive to a rack and finally via the tie rods and levers to the left and right front wheel. In this dissertation, the feedback actuator is also called FU motor, while the front axle actuator is called AU motor. In literature, the feedback actuator is also referred to as hand wheel actuator and the front axle actuator as road wheel actuator [48]. The FU model and the AU model are described in detail in [1] and Paper I.

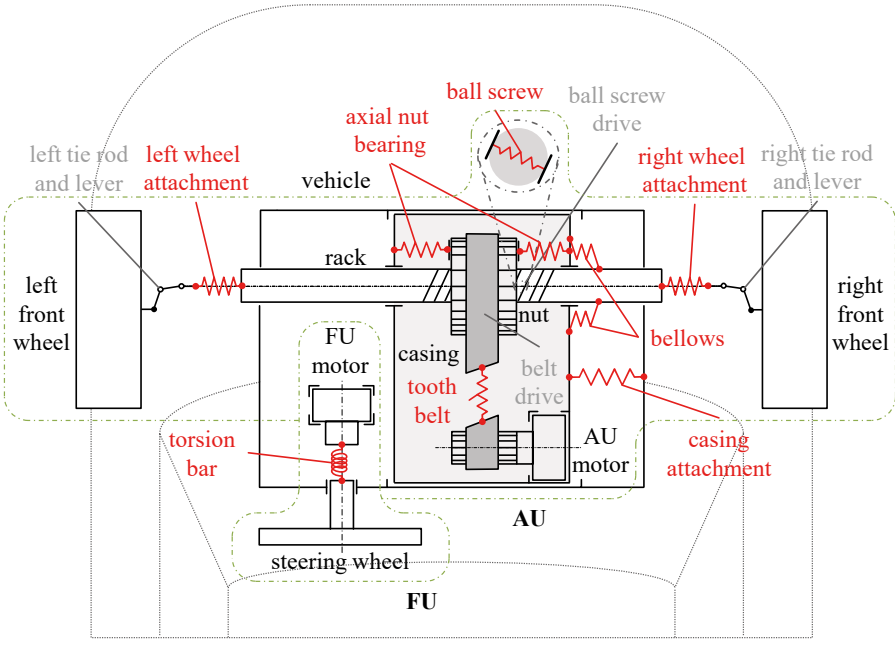

Figure 3.2. Physical substitute model of the SbW system with nine degrees of freedom.

The combination of the linearized detailed AU model with the corresponding FU model yields the linearized detailed SbW model with the state-space representation[1]

$$\begin{aligned} \dot{\underline{x}}_p(t) &= \underline{A}_p \underline{x}_p(t) + \underline{B}_{pc} \underline{u}_{pc}(t) + \underline{B}_{pd} \underline{u}_{pd}(t) \;\;,\;\; \underline{x}_p(0) = \underline{x}_{p,0} \\ \underline{y}_{po}(t) &= \underline{C}_{po} \underline{x}_p(t) \end{aligned} \qquad (3.1)$$

[1] Matrices are symbolized by upper-case letters with an underline, while vectors are symbolized by lower-case letters with an underline. Moreover, $\dot{x} = \mathrm{d}x/\mathrm{d}t$ denotes the time derivative of x.

This detailed SbW model is a reliable model of a real SbW system as the plant. It is therefore also called plant model. Here, $\underline{A}_p \in \mathbb{R}^{20x20}$ describes the system matrix, $\underline{B}_{pc} \in \mathbb{R}^{20x2}$ the control input matrix, $\underline{B}_{pd} \in \mathbb{R}^{20x2}$ the disturbance input matrix and $\underline{C}_{po} \in \mathbb{R}^{2x20}$ the objective output matrix of the plant model. Due to the actuator dynamics, the feedthrough matrix of the state-space representation is equal to a zero matrix and thus not displayed in Equation (3.1). Moreover, $\underline{x}_p(t) \in \mathbb{R}^{20}$ is the state vector and $\underline{x}_{p,0} \in \mathbb{R}^{20}$ the initial state vector of the plant model[2]. The state vector $\underline{x}_p$ contains the state variables of the model. Here, the individual mechanical degrees of freedom of the detailed SbW model and their time derivative as well as the motor torques were selected as state variables. Furthermore, $\underline{u}_{pc}(t) \in \mathbb{R}^2$ represents the control input vector, $\underline{u}_{pd}(t) \in \mathbb{R}^2$ the disturbance input vector and $\underline{y}_{po}(t) \in \mathbb{R}^2$ the objective output vector of the plant model. They are defined as

$$\underline{u}_{pc}(t) = \begin{bmatrix} T_{MF_{rq}}(t) \\ T_{MA_{rq}}(t) \end{bmatrix}, \quad \underline{u}_{pd}(t) = \begin{bmatrix} T_S(t) \\ F_R(t) \end{bmatrix}, \quad \underline{y}_{po}(t) = \begin{bmatrix} T_{TB}(t) \\ s_R(t) \end{bmatrix}. \tag{3.2}$$

The two variables T_{MFrq} and T_{MArq} within the control input vector $\underline{u}_{pc}$ describe the requested FU and AU motor torques for the subordinate torque control of the actuators integrated in the detailed SbW model [49]. They form the control variables of the plant model. In addition, the variables T_S and F_R within the disturbance input vector $\underline{u}_{pd}$ represent the disturbance variables of the plant model. The objective output vector $\underline{y}_{po}$ includes the torsion bar torque T_{TB} within the FU and the deflection s_R of the rack within the AU. They form the controlled variables of the plant model.

Further information regarding the development of the detailed SbW model as the plant model is given in [1] and Paper I. The methodology for modeling is also described in Paper IV and Paper VI.

3.2 Analysis of the Steer-by-Wire Model

The second step of the MDC is the analysis of the previously developed detailed SbW model as the plant model. This model serves as a representation of an actual SbW system. The objective of this model analysis is to gain a comprehensive understanding of the characteristics of a SbW system. This in-

[2] The time dependence of the vectors and physical quantities is explicitly denoted the first time they are mentioned. For every further mention, the time dependence is omitted for better readability.

cludes its structure, stability, deficiencies, parameter dependencies and sensitivities as well as its dominant behavior in both the time and frequency domain. This insight allows the development of specific approaches for the improvement of the characteristics of the SbW system and the realization of the predefined functional requirements. The parameterization of the model is derived from a representative steering system. The individual process steps from the model equations to the model characteristics are illustrated in Figure 3.3.

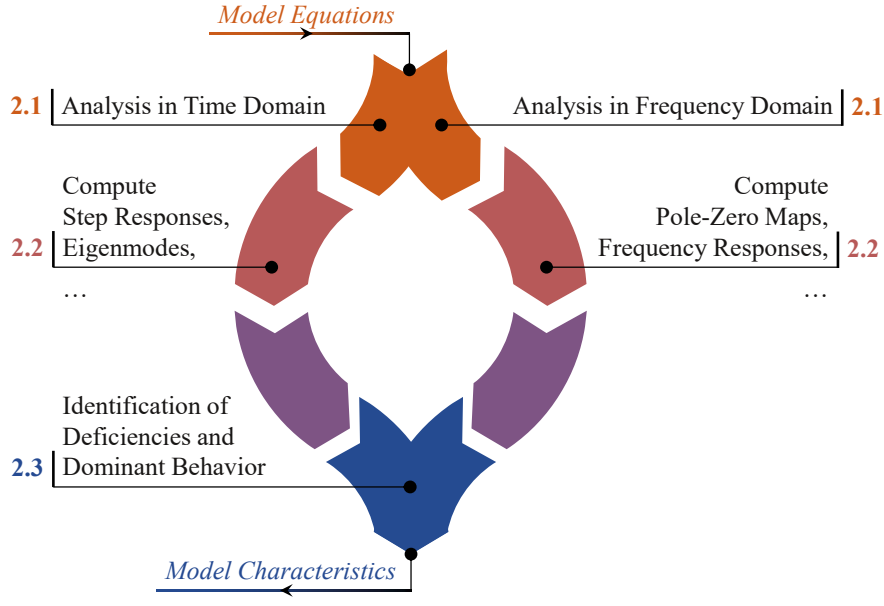

Figure 3.3. Process steps of the model analysis.

When the detailed SbW model from Equation (3.1) is analyzed in the time and frequency domain, it is evident that the FU model is dominated by a second order lag behavior. Conversely, the AU model is dominated by the superposition of an integral behavior, a first order lag behavior and a dominant second order lag behavior. [1] The second order lag behavior of the FU model depends on the stiffness c_{TB} of the torsion bar as well as on the moments of inertia J_S and J_{MF} of the steering wheel and the FU motor. The integral behavior of the AU model, including the first order lag behavior, results from the rigid body motion with viscous friction. The dominant second order lag behavior of the AU model depends mainly on the parameters of the front wheels and the wheel attachments. Further results of the analysis of the detailed SbW model can be found in [1] and Paper I.

4 Design of a Control for Steer-by-Wire Systems

The following chapter is adapted from the author's licentiate thesis [1].

The third step of the MDC is the control design. The objective of this step is to augment the SbW system by a control so that the corresponding control system exhibits optimal behavior and satisfies all functional requirements. To achieve this, the identified model characteristics from Chapter 3.2 are utilized. The individual process steps from the model characteristics to the control system are shown in Figure 4.1.

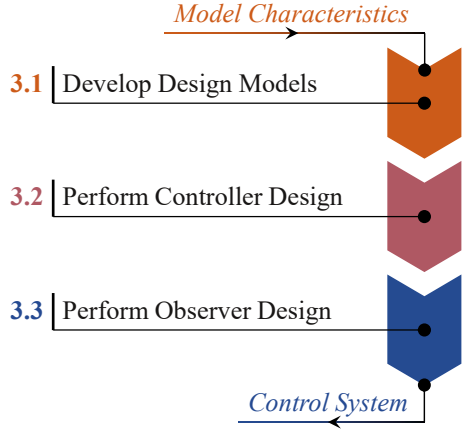

Figure 4.1. Process steps of the control design.

The controlled variables of the SbW system are the torsion bar torque T_{TB} within the FU and the deflection s_R of the rack within the AU. The corresponding reference variables depend on the respective driving situation. Hence, the requested torsion bar torque T_{TBrq} is mainly dependent on the rack force F_R and is calculated within the feeling generator. In contrast, the requested deflection s_{Rrq} of the rack depends on the steering wheel angle φ_S and is determined within a position generator. The parameterization of both the feeling

generator and the position generator results from the requirements of the SbW system. [1]

Current control approaches perform separate SISO control designs for the torsion bar torque T_{TB} and the deflection s_R of the rack. The corresponding separately designed control systems are combined via the feeling generator and the position generator. However, this causes shifts of the eigenvalues and alterations of the dynamic behavior (time and frequency responses), so that the supposed high robustness achieved by the respective design can no longer be guaranteed. [1] To address this issue, this chapter introduces a novel multivariable control approach that guarantees improved robustness of the controlled SbW system. For this, a state-space controller is designed, since it yields better results than classical controllers such as PID controllers or cascade controllers, as demonstrated in [16]. Further information regarding robust control design can be found in [50]-[54].

4.1 Development of an Optimal Design Model

The control system must satisfy the requirements of good control and disturbance behavior. In addition, it must have a high degree of robustness against unconsidered eigenmodes and parameter uncertainties in the plant model. For example, the rise time should be less than 0.1 s and the settling time should be less than 0.2 s with a maximum transient overshoot of 10 % in the case of step-shaped reference excitation. A small residual control error is acceptable, since steady-state accuracy is not mandatory for this application. Furthermore, the system response to sinusoidal excitations up to 100 rad/s (16 Hz) should not deviate by more than 20 % from the amplitude of the excitation, since the driver is particularly sensitive in this frequency range. [1] A prerequisite for this required good dynamic behavior is active vibration damping of the oscillating modes of the SbW system. Therefore, a linear-quadratic-Gaussian (LQG) compensator is designed which considers the natural limitations of the real system, ensuring that no bounds are exceeded during normal operation. However, using a high-order model for the compensator (controller and observer) design poses challenges because its parameters are often difficult to identify or vary substantially during operation. This is detrimental to the control, since it does not match the respective eigenmodes of the plant sufficiently. Consequently, a compensator of the lowest possible order should be implemented. Nonetheless, the design model should not be reduced too much to ensure that all dominant characteristics of the plant are represented. Hence,

an optimally reduced plant model is derived, serving as the basis for the subsequent compensator design. The starting point is the linearized detailed SbW model from Chapter 3.1, consisting of the FU and AU model. [1]

The mechanical part of the FU model has two degrees of freedom and corresponds to a two-mass oscillator. Thus, it already is a model of low order and does not need to be reduced any further in this application. However, the mechanical part of the AU model has seven degrees of freedom and therefore a correspondingly high order. In addition, it has high-frequency characteristics. Hence, it needs to be reduced. Real system excitations can have frequencies up to 190 rad/s (30 Hz) [16]. Consequently, it is crucial that the reduced AU model aligns well with the detailed AU model up to this frequency. As identified in [1], the eigenfrequencies due to the elastic wheel attachment within the AU are about 150 rad/s (24 Hz). Accordingly, the reduced AU model should consider these elastic elements, while the remaining elastic elements can be neglected, since the associated eigenfrequencies are much larger than 190 rad/s (30 Hz). Figure 4.2 shows the frequency response of the control transfer path of the resulting AU model. For comparison, the frequency response of the control transfer path of the detailed AU model is also depicted in this figure.

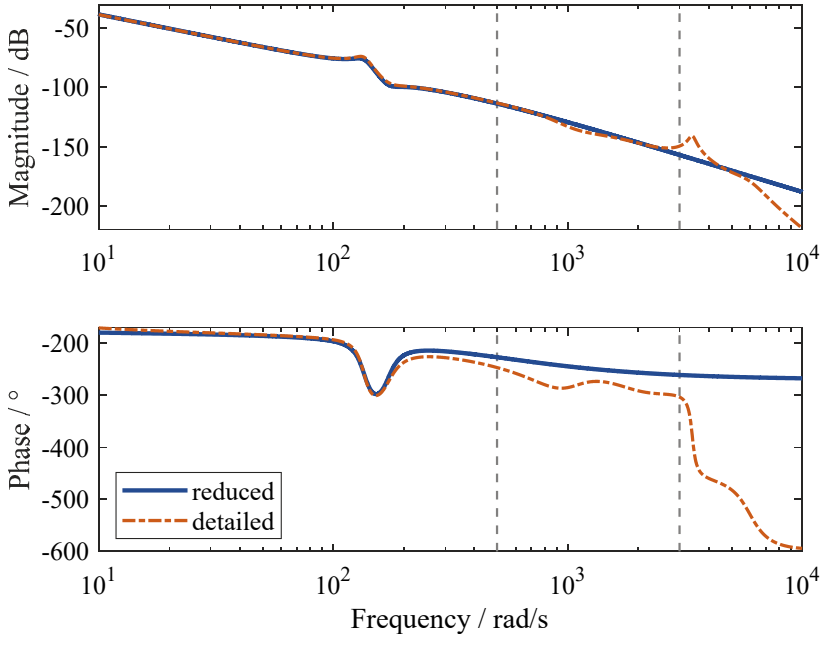

Figure 4.2. Frequency response of the control transfer path of the reduced AU model (blue) and detailed AU model (orange) from the requested AU motor torque $T_{MA_{rq}}$ to the deflection s_R of the rack.

The detailed AU model consists of a mechanical model with seven degrees of freedom, while the reduced AU model consists of a mechanical model with two degrees of freedom, both coupled with a torque control for the AU motor. It can be seen that the developed reduced AU model maps the magnitude response of the detailed AU model with sufficient accuracy up to frequencies of 3000 rad/s (480 Hz) and the phase response up to frequencies of 500 rad/s (80 Hz). Consequently, the reduced AU model is suitable for the control design. The sufficient correspondence between the reduced model and the detailed model can also be observed by analyzing the eigenmodes of the two models. The eigenmodes as well as further analysis results of the reduced model can be found in Paper I.

Combining the reduced AU model with the FU model generates the reduced SbW model resp. reduced plant model with the state-space representation

$$\begin{aligned} \dot{\underline{x}}_{\tilde{p}}(t) &= \underline{A}_{\tilde{p}}\underline{x}_{\tilde{p}}(t) + \underline{B}_{\tilde{p}c}\underline{u}_{pc}(t) + \underline{B}_{\tilde{p}d}\underline{u}_{pd}(t) \;,\; \underline{x}_{\tilde{p}}(0) = \underline{x}_{\tilde{p},0} \\ \underline{y}_{po}(t) &\approx \underline{C}_{\tilde{p}o}\underline{x}_{\tilde{p}}(t) \end{aligned} \;, \tag{4.1}$$

where the reduced plant model still has the same input and output vectors $\underline{u}_{pc}$, $\underline{u}_{pd}$ and $\underline{y}_{po}$ as the detailed plant model according to Equation (3.2). Moreover, $\underline{A}_{\tilde{p}} \in \mathbb{R}^{10\text{x}10}$ represents the system matrix, $\underline{B}_{\tilde{p}c} \in \mathbb{R}^{10\text{x}2}$ the control input matrix, $\underline{B}_{\tilde{p}d} \in \mathbb{R}^{10\text{x}2}$ the disturbance input matrix and $\underline{C}_{\tilde{p}o} \in \mathbb{R}^{2\text{x}10}$ the objective output matrix of the reduced plant model. Like the detailed plant model, the reduced plant model has a feedthrough matrix equal to a zero matrix, so that the feedthrough matrix of the reduced plant model is neglected in Equation (4.1). Furthermore, $\underline{x}_{\tilde{p}}(t) \in \mathbb{R}^{10}$ is the state vector and $\underline{x}_{\tilde{p},0} \in \mathbb{R}^{10}$ the initial state vector of the reduced plant model. This reduced plant model, consisting of the FU model and the reduced AU model, answers the first research question from Chapter 1.1 in an optimal way. Therefore, it is used for the subsequent control design.

4.2 Direct Discrete Controller Design

The developed reduced SbW model is a suitable approximation of a real SbW system. It serves as the plant model for the design of a novel discrete LQG compensator. This compensator encompasses a discrete linear optimal static state-space controller and a discrete linear optimal state-space observer. The linear optimal state-space controller is also called linear-quadratic regulator (LQR), while the linear optimal state-space observer is also called linear-

quadratic estimator (LQE). Figure 4.3 illustrates the block diagram of the discrete closed-loop system consisting of the resulting discrete LQG compensator and a plant model with zero-order-hold (zoh) element. In this context, $\underline{\hat{x}}_{p,k} \in \mathbb{R}^{np}$ and $\underline{\hat{x}}_{d,k} \in \mathbb{R}^{pd}$ represent the a-posteriori estimates of the state vector and the disturbance input vector of the plant model with the number n_p of state variables and the number p_d of disturbance input variables of the plant model. Moreover, $\underline{u}_{pc,k} \in \mathbb{R}^{pc}$ and $\underline{u}_{pd,k} \in \mathbb{R}^{pd}$ describe the control and disturbance input vector of the plant model with the number p_c of control input variables of the plant model. The vectors $\underline{y}_{pm,k} \in \mathbb{R}^{qm}$ and $\underline{y}_{po,k} \in \mathbb{R}^{qo}$ denote the measurement and objective output vector of the plant model with the number q_m of measurement output variables and the number q_o of objective output variables of the plant model. Additionally, $\underline{x}_{r,k} \in \mathbb{R}^{qo}$ represents the reference vector of the discrete LQG compensator, which in general summarizes the reference variables. However, since a model of the reference variables is included in the following LQR design, the reference vector $\underline{x}_{r,k}$ must only contain the deviation of the reference variables from the operating point considered in the LQR design. Therefore, the reference vector $\underline{x}_{r,k}$ is displayed in gray in Figure 4.3. [1]

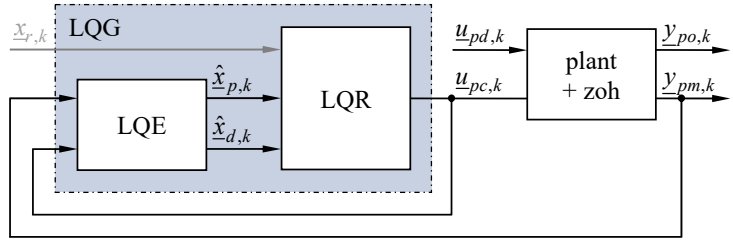

Figure 4.3. Block diagram of the discrete closed-loop system with discrete LQG compensator.

The task of the LQR within the compensator is to adjust the torsion bar torque T_{TB} and the deflection s_R of the rack to their respective requested values T_{TBrq} and s_{Rrq}. For this, the requested FU and AU motor torques T_{MFrq} and T_{MArq} are the control variables. The steering torque T_S and the rack force F_R act as disturbance variables for the control system. The effect of these disturbance variables on the controlled variables T_{TB} and s_R is compensated by a disturbance feedforward.

The design of the LQR uses the reduced plant model from Chapter 4.1 as the plant model, assuming that all its state and disturbance variables are measurable or observable. For this LQR design, the plant model is augmented by a suitable linear reference and disturbance model as well as a weighting model, so that an augmented plant model is obtained as the design model. Figure 4.4 shows the block diagram of this augmented plant model. There, no noise is

displayed, as it has no effect on the result of the LQR design. The reference model determines the reference variables as a function of the state and disturbance variables of the plant model. It consists of the linearized feeling generator and the position generator. The feeling generator computes the requested torsion bar torque T_{TBrq}, which serves as a substitute for the requested steering torque to provide the driver with feedback on the current driving situation. In addition, the position generator calculates the requested deflection s_{Rrq} of the rack depending on the current steering wheel angle φ_S. Furthermore, the weighting model provides the control error $e_{TTB} = T_{TBrq} - T_{TB}$ of the torsion bar torque as well as the control error $e_{sR} = s_{Rrq} - s_R$ of the deflection of the rack as the design objectives.

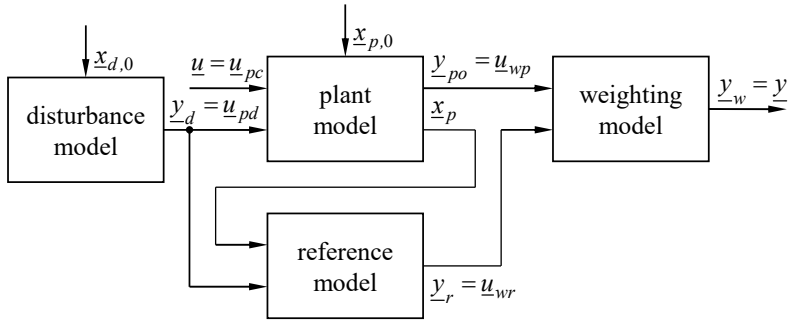

Figure 4.4. Block diagram of the augmented plant model for the LQR design.

The coupling of these models, as illustrated in Figure 4.4, results in the augmented plant model for the LQR design. The main variables of the augmented plant model are described in Table 4.1.

Table 4.1. Variables of the block diagram of the augmented plant model for the LQR design.

Symbol	Description
$\underline{u}$	input vector of the augmented plant model
$\underline{u}_{pc}$	control input vector of the plant model
$\underline{u}_{pd}$	disturbance input vector of the plant model
$\underline{u}_{wp}$	plant input vector of the weighting model
$\underline{u}_{wr}$	reference input vector of the weighting model
$\underline{x}_{d,0}$	initial state vector of the disturbance model
$\underline{x}_p$	state vector of the plant model
$\underline{x}_{p,0}$	initial state vector of the plant model
$\underline{y}$	output vector of the augmented plant model
$\underline{y}_d$	output vector of the disturbance model
$\underline{y}_{po}$	objective output vector of the plant model
$\underline{y}_r$	output vector of the reference model
$\underline{y}_w$	output vector of the weighting model

For the direct discrete LQR design, it is necessary to discretize the augmented plant model by performing the step-invariant discretization. The discretization transforms the continuous augmented plant model according to Figure 4.4 into a discrete model with the discrete state-space representation[3]

$$\begin{aligned} \underline{x}_{k+1} &= \underline{A}_D\,\underline{x}_k + \underline{B}_D\,\underline{u}_k \\ \underline{y}_k &= \underline{C}_D\,\underline{x}_k + \underline{D}_D\,\underline{u}_k \end{aligned} \quad , \tag{4.2}$$

where the system matrix of the discretized augmented plant model is denoted by $\underline{A}_D \in \mathbb{R}^{nxn}$, the input matrix by $\underline{B}_D \in \mathbb{R}^{nxp}$, the output matrix by $\underline{C}_D \in \mathbb{R}^{qxn}$ and the feedthrough matrix by $\underline{D}_D \in \mathbb{R}^{qxp}$, with the number n of state variables, the number p of input variables and the number q of output variables of the discrete augmented plant model. Since the feedthrough matrix of the continuous plant model according to equation (4.1) is equal to a zero matrix, the feedthrough matrix $\underline{D}_D$ of the discrete augmented plant model for the LQR design after step-invariant discretization is also equal to a zero matrix. Nevertheless, a general derivation of the LQR design shall be presented in this chapter, so that the feedthrough matrix $\underline{D}_D$ is included in Equation (4.2) and the following equations. Further information regarding discretization can be found in [55]. Moreover, the input vector $\underline{u}_k \in \mathbb{R}^p$ of the discrete augmented plant model is equal to the control input vector $\underline{u}_{pc,k}$ of the discrete plant model ($p = p_c$), whereas the output vector $\underline{y}_k = \underline{x}_{r,k} - \underline{y}_{po,k} \in \mathbb{R}^q$ of the discrete augmented plant model summarizes the control errors ($q = q_o$). In addition, $\underline{x}_k \in \mathbb{R}^n$ describes the state vector and $\underline{x}_0 \in \mathbb{R}^n$ the initial state vector of the discrete augmented plant model for the LQR design.

For this discrete model, an optimal state-space controller with the control law

$$\underline{u}_k = -\underline{K}\underline{x}_k \tag{4.3}$$

and

$$\underline{K} = (\underline{R} + \underline{D}_D^T \underline{Q} \underline{D}_D + \underline{B}_D^T \underline{S} \underline{B}_D)^{-1} (\underline{B}_D^T \underline{S} \underline{A}_D + \underline{D}_D^T \underline{Q} \underline{C}_D) \tag{4.4}$$

[3] State-space matrices of a discrete model are symbolized by an index D. The corresponding sequence of vectors $\underline{x}_k := \underline{x}(kT)$ is symbolized by an index k for characterizing the point in time kT with $k \in \mathbb{N}_0$ and the sample time T.

is designed. Here, $\underline{K} \in \mathbb{R}^{pxn}$ is the optimal LQR gain matrix and $\underline{S} \in \mathbb{R}^{nxn}$ is the matrix that represents the positive definite solution of the associated algebraic matrix Riccati equation

$$\begin{aligned} &\underline{A}_D^T \underline{S} \underline{A}_D - (\underline{A}_D^T \underline{S} \underline{B}_D + \underline{C}_D^T \underline{\underline{Q}} \underline{D}_D)(\underline{R} + \underline{D}_D^T \underline{\underline{Q}} \underline{D}_D \\ &\quad + \underline{B}_D^T \underline{S} \underline{B}_D)^{-1} (\underline{B}_D^T \underline{S} \underline{A}_D + \underline{D}_D^T \underline{\underline{Q}} \underline{C}_D) - \underline{S} + \underline{C}_D^T \underline{\underline{Q}} \underline{C}_D = \underline{0} \end{aligned} \quad , \tag{4.5}$$

where $\underline{R} \in \mathbb{R}^{pxp}$ and $\underline{\underline{Q}} \in \mathbb{R}^{qxq}$ are the positive (semi-)definite weighting matrices[4]. They are the design parameters. The weighting matrix $\underline{R}$ penalizes the use of control variables, whereas the weighting matrix $\underline{\underline{Q}}$ penalizes control errors. A pragmatic and physically appropriate choice is to set the elements of $\underline{R}$ and $\underline{\underline{Q}}$ equal to the reciprocal values of the corresponding maximum allowed variances [1][56]. A detailed description of the continuous control design is documented in Paper II, while the direct discrete design is presented in Paper III. This paper also describes the selection of a suitable discretization method. Furthermore, the methodology for the optimal control design is also described in Paper IV.

4.3 Direct Discrete Observer Design

Within the LQR, the state and disturbance variables of the plant model are fed back. Since not all of them are measurable, an LQE is designed in this chapter to provide optimal estimates for the state and disturbance variables of the plant model. The starting point for the LQE design is again the reduced plant model from Chapter 4.1. This model is augmented by an integrator disturbance model to enable the estimation of disturbances [1][56]. Accordingly, the disturbance variables of the plant model are state variables of the disturbance model. Figure 4.5 illustrates the block diagram of the resulting augmented plant model in a mixed deterministic and stochastic environment.

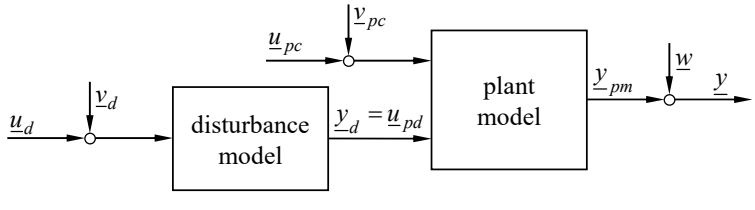

Figure 4.5. Block diagram of the augmented plant model for the LQE design.

[4] $\underline{0}$ symbolizes a zero matrix and $\underline{I}$ an identity matrix of corresponding size.

The main variables of the augmented plant model for the LQE design are described in Table 4.2.

Table 4.2. Variables of the block diagram of the augmented plant model for the LQE design.

Symbol	Description
$\underline{u}_d$	input vector of the disturbance model
$\underline{u}_{pc}$	control input vector of the plant model
$\underline{u}_{pd}$	disturbance input vector of the plant model
$\underline{v}_d$	vector of process noise for the disturbance model
$\underline{v}_{pc}$	vector of process noise for the plant model
$\underline{w}$	vector of measurement noise for the plant model
$\underline{y}$	output vector of the augmented plant model
$\underline{y}_d$	output vector of the disturbance model
$\underline{y}_{pm}$	measurement output vector of the plant model

For the direct discrete LQE design, the augmented plant model is discretized partly step-invariant and partly impulse-invariant, so that the discrete augmented plant model with the discrete state-space representation

$$\begin{aligned} \underline{x}_{k+1} &= \underline{A}_D\,\underline{x}_k + \underline{B}_D\,\underline{u}_k + \underline{F}_D\,\underline{v}_k \\ \underline{y}_k &= \underline{C}_D\,\underline{x}_k + \underline{D}_D\,\underline{u}_k + \underline{w}_k \end{aligned} \tag{4.6}$$

results. This representation includes the system matrix $\underline{A}_D \in \mathbb{R}^{n\mathrm{x}n}$, the input matrix $\underline{B}_D \in \mathbb{R}^{n\mathrm{x}p}$, the output matrix $\underline{C}_D \in \mathbb{R}^{q\mathrm{x}n}$ and the feedthrough matrix $\underline{D}_D \in \mathbb{R}^{q\mathrm{x}p}$ of the discrete augmented plant model for the LQE design[5]. Due to the partly step-invariant and partly impulse-invariant discretization, the feedthrough matrix $\underline{D}_D$ of the discrete augmented plant model for the LQE design is unequal to a zero matrix, although the continuous plant model according to Equation (4.1) has a feedthrough matrix equal to a zero matrix. Moreover, $\underline{v}_k = [\underline{v}_{pc,k}, \underline{v}_{d,k}]^{\mathrm{T}} \in \mathbb{R}^p$ describes the vector of process noise and $\underline{F}_D \in \mathbb{R}^{n\mathrm{x}p}$ the noise filter matrix for the process noise as well as $\underline{w}_k \in \mathbb{R}^q$ the vector of measurement noise for the discrete augmented plant model. Furthermore, the input vector $\underline{u}_k = [\underline{u}_{pc,k}, \underline{u}_{d,k}]^{\mathrm{T}} \in \mathbb{R}^p$ of the discrete augmented plant model now combines the control input vector $\underline{u}_{pc,k}$ of the discrete plant model and the input vector $\underline{u}_{d,k}$ of the discrete disturbance model ($p = p_c + p_d$). The state vector $\underline{x}_k = [\underline{x}_{p,k}, \underline{x}_{d,k}]^{\mathrm{T}} \in \mathbb{R}^n$ of the discrete augmented plant model unifies the state vector $\underline{x}_{p,k}$ and the disturbance input vector $\underline{x}_{d,k}$ of the discrete plant model ($n = n_p + p_d$). Additionally, the output vector $\underline{y}_k = \underline{y}_{pm,k} + \underline{w}_k \in \mathbb{R}^q$ is equal to the

[5] The state-space matrices from Equation (4.2) are unequal to the state-space matrices from Equation (4.6). Nevertheless, the same identifiers are used here to simplify the subsequent equations.

measurement output vector $\underline{y}_{pm,k}$ of the discrete plant model ($q = q_m$) including the vector of $\underline{w}_k$ measurement noise.

The objective of the direct discrete LQE design is to develop an observer that provides optimal estimates of the state vector $\underline{x}_k$ of the discrete augmented plant model in the presence of process and measurement noise. For the discrete LQE, the discrete state-space representation

$$\begin{aligned} \underline{\tilde{x}}_{k+1} &= \underline{A}_D \underline{\hat{x}}_k + \underline{B}_D \underline{u}_k \quad , \quad \underline{\tilde{x}}_0 = \underline{0} \\ \underline{\tilde{y}}_k &= \underline{C}_D \underline{\tilde{x}}_k + \underline{D}_D \underline{u}_k \\ \underline{\hat{x}}_k &= \underline{\tilde{x}}_k + \underline{\hat{K}} (\underline{y}_k - \underline{\tilde{y}}_k) \end{aligned} \tag{4.7}$$

is defined, where $\underline{\tilde{x}}_k = [\underline{\tilde{x}}_{p,k}, \underline{\tilde{x}}_{d,k}]^T \in \mathbb{R}^n$ and $\underline{\hat{x}}_k = [\underline{\hat{x}}_{p,k}, \underline{\hat{x}}_{d,k}]^T \in \mathbb{R}^n$ denote the a-priori and a-posteriori estimates of the state vector $\underline{x}_k$ of the discrete augmented plant model as well as $\underline{\tilde{y}}_k \in \mathbb{R}^q$ the estimate of the noisy measurement output vector $\underline{y}_k = \underline{y}_{pm,k} + \underline{w}_k$ of the discrete plant model. Moreover, $\underline{\tilde{x}}_{p,k}$ and $\underline{\hat{x}}_{p,k}$ describe the a-priori and a-posteriori estimate of the state variables of the discrete plant model, while $\underline{\tilde{x}}_{d,k}$ and $\underline{\hat{x}}_{d,k}$ represent the a-priori and a-posteriori estimate of the disturbance variables of the discrete plant model. The optimal LQE gain matrix is represented by $\underline{\hat{K}} \in \mathbb{R}^{nxq}$. Through reformulation, the discrete state-space representation

$$\begin{aligned} \underline{\tilde{x}}_{k+1} &= \underline{A}_D (\underline{I} - \underline{\hat{K}} \underline{C}_D) \underline{\tilde{x}}_k + \begin{bmatrix} \underline{B}_D - \underline{A}_D \underline{\hat{K}} \underline{D}_D & \underline{A}_D \underline{\hat{K}} \end{bmatrix} \begin{bmatrix} \underline{u}_k \\ \underline{y}_k \end{bmatrix} \\ \underline{\hat{x}}_k &= (\underline{I} - \underline{\hat{K}} \underline{C}_D) \underline{\tilde{x}}_k + \begin{bmatrix} -\underline{\hat{K}} \underline{D}_D & \underline{\hat{K}} \end{bmatrix} \begin{bmatrix} \underline{u}_k \\ \underline{y}_k \end{bmatrix} \end{aligned} \tag{4.8}$$

of the LQE with

$$\underline{\hat{K}} = \underline{\tilde{P}} \underline{C}_D^T (\underline{C}_D \underline{\tilde{P}} \underline{C}_D^T + \underline{W})^{-1} \tag{4.9}$$

is obtained. Here, $\underline{\tilde{P}} \in \mathbb{R}^{nxn}$ is the stationary covariance matrix of the a-priori estimation error. It is the positive definite solution of the associated algebraic matrix Riccati equation

$$\begin{aligned} \underline{A}_D \underline{\tilde{P}} \underline{A}_D^T - \underline{A}_D \underline{\tilde{P}} \underline{C}_D^T (\underline{C}_D \underline{\tilde{P}} \underline{C}_D^T + \underline{W})^{-1} \underline{C}_D \underline{\tilde{P}} \underline{A}_D^T - \underline{\tilde{P}} \\ + \underline{F}_D \underline{V} \underline{F}_D^T = \underline{0} \end{aligned} \quad . \tag{4.10}$$

The positive (semi-)definite intensity matrices $\underline{V} \in \mathbb{R}^{pxp}$ and $\underline{W} \in \mathbb{R}^{qxq}$ of the process and measurement noise act as the design parameters. They are similar to the weighting matrices $\underline{R}$ and $\underline{Q}$ in the LQR design. The intensity matrix $\underline{V}$ of the process noise penalizes the use of the control variables of the discrete plant model, while the intensity matrix $\underline{W}$ of the measurement noise penalizes using the measurement output variables of the discrete plant model for estimating the state vector $\underline{x}_k$ of the discrete augmented plant model. [1] Suitable elements for the intensity matrices $\underline{V}$ and $\underline{W}$ are outlined in [56].

Since the disturbance model is not present in reality and measurement noise is inherently integrated in the measurement output vector $\underline{y}_{pm,k}$ of the plant model, the LQE from Equation (4.8) is realized with the discrete state-space representation

$$\begin{aligned} \tilde{\underline{x}}_{k+1} &= \underline{A}_D(\underline{I} - \hat{\underline{K}}\underline{C}_D)\tilde{\underline{x}}_k + \begin{bmatrix} \underline{B}_{c_D} - \underline{A}_D\hat{\underline{K}}\underline{D}_{c_D} & \underline{A}_D\hat{\underline{K}} \end{bmatrix} \begin{bmatrix} \underline{u}_{pc,k} \\ \underline{y}_{pm,k} \end{bmatrix} \\ \hat{\underline{x}}_k &= (\underline{I} - \hat{\underline{K}}\underline{C}_D)\tilde{\underline{x}}_k + \begin{bmatrix} -\hat{\underline{K}}\underline{D}_{c_D} & \hat{\underline{K}} \end{bmatrix} \begin{bmatrix} \underline{u}_{pc,k} \\ \underline{y}_{pm,k} \end{bmatrix} \end{aligned}, \qquad (4.11)$$

where $\underline{B}_{cD}$ denotes the control input matrix and $\underline{D}_{cD}$ the control feedthrough matrix of the discrete augmented plant model for the LQE design. The block diagram of the resulting discrete LQE is depicted in Figure 4.6[6].

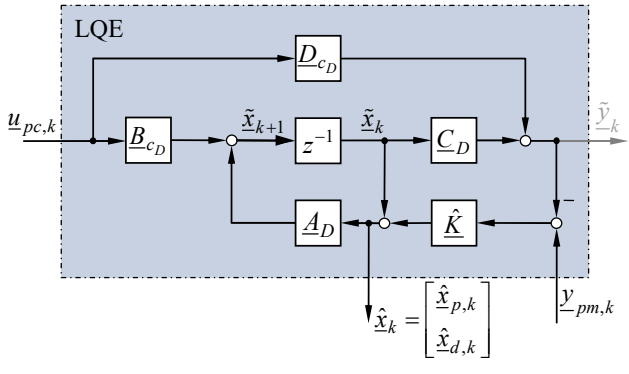

Figure 4.6. Block diagram of the discrete LQE.

Since in this application only the a-posteriori estimate $\hat{\underline{x}}_k$ of the state vector $\underline{x}_k$ of the discrete augmented plant model is required as output of the discrete

[6] z^{-1} describes the right shift of a sequence according to the z-transform.

LQE, the estimate $\tilde{\underline{y}}_k$ of the measurement output vector is shown in gray in Figure 4.6.

A detailed description of the performed direct discrete design is provided in Paper III.

5 Analysis of the Controlled Steer-by-Wire System

The following chapter is adapted from the author's licentiate thesis [1].

The fourth step of the MDC is the system analysis. This step analyzes whether the designed control satisfies all specified requirements. In this application, the control system consists of the detailed SbW model from Chapter 3.1, which accurately represents the real plant, and the control algorithm designed in Chapter 4 utilizing the reduced SbW model. This enables the analysis of the robustness of the control system against eigenmodes of the real SbW system that were not considered in the design model. The system analysis is conducted comprehensively in both the time and frequency domain. The corresponding process steps are depicted in Figure 3.3. [1]

To simulate real driving situations, the control system is augmented by a vehicle dynamics (VD) model as well as a driver actuation (DA) model [57]. Figure 5.1 shows the block diagram of the corresponding discrete control system in this augmented simulation environment. Here, a reference generator is depicted within the control algorithm. Since a reference model has been included in the LQR design, the reference generator must only compute the deviation of the reference variables from the operating point considered in the LQR design. Therefore, the reference generator is displayed in gray in Figure 5.1.

The input variables of the VD model are the drive torque T_D generated by the combustion engine or electric motor of the vehicle as well as the vector $\underline{\mu}$ of friction coefficients between the tires of the vehicle and the road. Based on these variables plus the steering angles φ_{WL} and φ_{WR} as well as the angular velocities Ω_{WL} and Ω_{WR} of the front wheels, the VD model computes the torques T_{WL} and T_{WR} about the steering axis of the left and right front wheel, which are aggregated and transformed into an equivalent rack force F_R as an output variable of the VD model. In contrast, the input variables of the DA model are the requested steering wheel angle φ_{Srq} that the driver has to set to follow a desired trajectory, the actual steering wheel angle φ_S and the angular velocity Ω_S of the steering wheel. Then, the developed DA model determines

the steering torque T_S that the driver induces at the steering wheel. A detailed description of these models is given in the following sections.

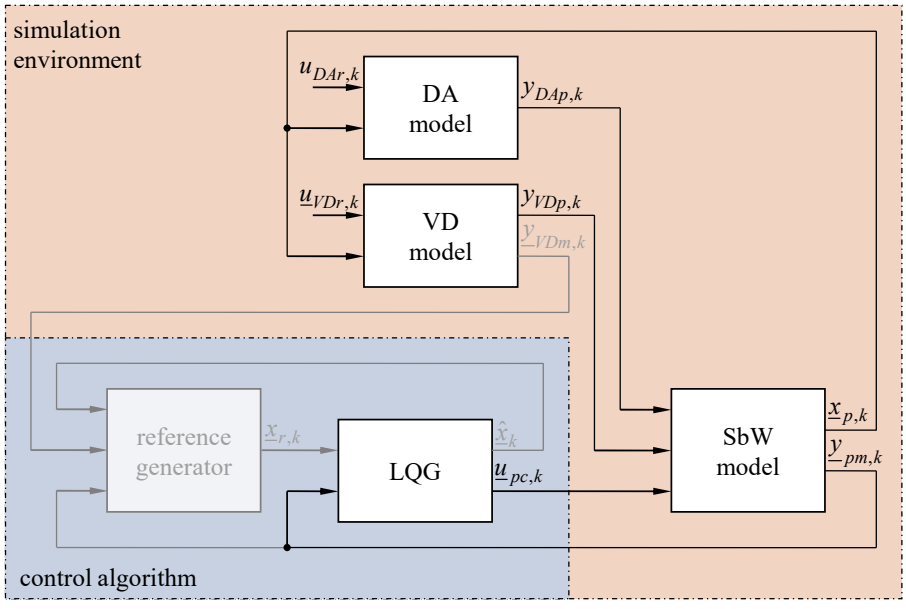

Figure 5.1. Block diagram of the discrete augmented control system.

The main variables of the discrete augmented control system are described in Table 5.1[7].

Table 5.1. Variables of the block diagram of the discrete augmented control system.

Symbol	Description
$u_{DAr,k}$	reference input variable of the discrete DA model
$\underline{u}_{pc,k}$	control input vector of the discrete detailed SbW model
$\underline{u}_{VDr,k}$	reference input vector of the discrete VD model
$\hat{\underline{x}}_k$	a-posteriori estimate of the state vector of the discrete augmented plant model for the LQE design
$\underline{x}_{p,k}$	state vector of the discrete detailed SbW model
$\underline{x}_{r,k}$	reference vector of the discrete LQG compensator
$y_{DAp,k}$	plant output variable of the discrete DA model
$\underline{y}_{pm,k}$	measurement output vector of the discrete detailed SbW model
$\underline{y}_{VDm,k}$	measurement output vector of the discrete VD model
$y_{VDp,k}$	plant output variable of the discrete VD model

[7] Here, $u_{DAr,k} = \varphi_{Srq,k}$, $\underline{u}_{VDr,k} = [T_{D,k}, \underline{\mu}_k]^T$, $y_{DAp,k} = T_{S,k}$, $y_{VDp,k} = F_{R,k}$ applies. Moreover, $\varphi_{S,k}$, $\varphi_{WL,k}$, $\varphi_{WR,k}$, $\Omega_{S,k}$, $\Omega_{WL,k}$ and $\Omega_{WR,k}$ are elements of the vector $\underline{x}_{p,k}$. For better readability, the index k is omitted for the physical quantities in the main text.

5.1 Development of a Vehicle Dynamics Model

The detailed SbW model includes the rack force F_R as input variable, based on the torques T_{WL} and T_{WR} about the steering axes of the front wheels. To compute this force realistically, a multibody model of a vehicle with tire models is required. Here, a simple two-track multibody model of a vehicle is used which consists of five rigidly coupled bodies. The corresponding physical substitute model is depicted in Figure 5.2. The individual rigid bodies are labelled with the indices CoG (center of gravity), WFL (left front wheel), WFR (right front wheel), WRL (left rear wheel) and WRR (right rear wheel). The degrees of freedom are indicated by blue arrows in Figure 5.2 and the remaining kinematic variables by orange arrows. An overview of the variables of the physical substitute model is provided in Table 5.2. For this model, the equations of motion have been derived. [58]

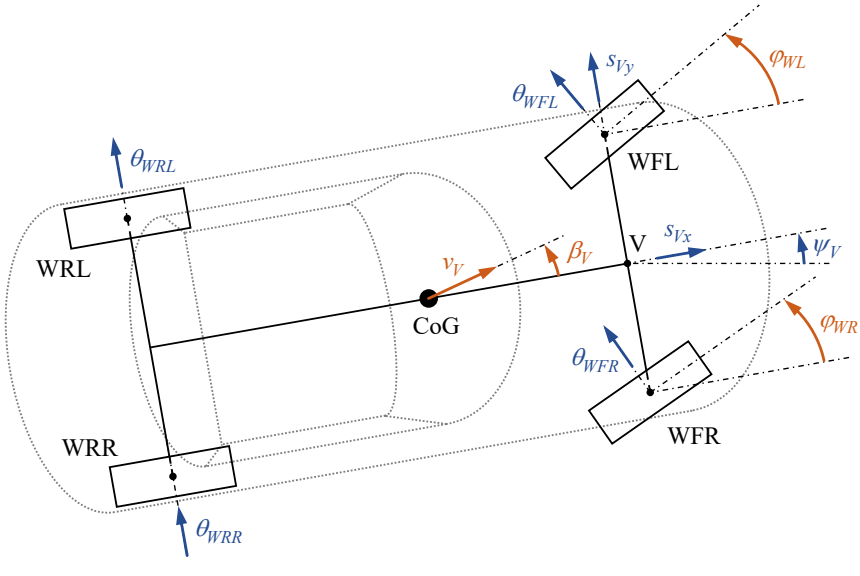

Figure 5.2. Physical substitute model of the vehicle.

The resulting multibody model of the vehicle possesses seven degrees of freedom: Three degrees of freedom account for the general deflection and rotation of the vehicle and four degrees of freedom for the rotation of the wheels. The steering mechanism of the front axle is not included in this multibody model of the vehicle because it is already considered in the SbW model. Hence, the steering angles φ_{WL} and φ_{WR} of the front wheels as well as their derivatives represent input variables of the multibody model of the vehicle.

Table 5.2. Variables of the physical substitute model of the vehicle.

Symbol	Description
s_{V_x}	translational degree of freedom in x-direction of the vehicle
s_{V_y}	translational degree of freedom in y-direction of the vehicle
v_V	translational vehicle velocity
β_V	side slip angle of the vehicle
θ_{WFL}	rotational degree of freedom of the left front wheel
θ_{WFR}	rotational degree of freedom of the right front wheel
θ_{WRL}	rotational degree of freedom of the left rear wheel
θ_{WRR}	rotational degree of freedom of the right rear wheel
φ_{WL}	steering angle of the left front wheel
φ_{WR}	steering angle of the right front wheel
ψ_V	yaw angle of the vehicle

The drive torque T_D is also an input variable of the multibody model of the vehicle. In addition, forces and torques act on the wheels due to the road contact. They can be calculated for a given driving situation using tire models. The tires characterize the connection between the vehicle and the road. They generate forces and torques and increase the driving comfort by compensating road unevenness. The increase in comfort is based on the ability of a tire to deform. This deformability as well as the construction out of different materials results in a strongly nonlinear behavior. It can be modeled by different approaches. The tire model used here is based on the semi-empirical model TMEASY developed in [21]. The model incorporates the static behavior of a tire derived from empirical measurements and includes discrete elements such as springs and dampers to emulate the dynamic behavior of a tire.

The translational and angular velocity of a wheel are the input variables of the corresponding tire model. These velocities are output variables of the multibody model of the vehicle. Each tire model determines the forces and torques acting at the contact point between the respective wheel and the road. These tire forces and torques are fed back to the multibody model of the vehicle. Consequently, the torques T_{WL} and T_{WR} about the steering axes of the front wheels are resolved from these tire forces and torques. The torques T_{WL} and T_{WR} are aggregated and transformed to the rack force F_R, which is fed back to the SbW model.

The combination of the multibody model of the vehicle and the tire models builds the VD model. A detailed description of the VD model is provided in Paper IV. In the following, its parameterization corresponds to an average-sized car.

5.2 Development of a Driver Actuation Model

In order to control the lateral motion of a vehicle, the driver performs sensory and actuator tasks as well as control tasks: The driver perceives the current lateral motion of the vehicle, typically via the eyes, and influences it via the steering wheel angle φ_S. Consequently, the driver plays an important role in controlling the lateral motion of a vehicle and must be considered in the development, optimization and evaluation of steering systems.

Based on experience and a basic feeling for the driving dynamics of a vehicle, the driver is able to determine the requested steering wheel angle φ_{Srq} for a desired lateral motion of the vehicle. The driver then applies a steering torque T_S at the steering wheel to influence the steering wheel angle φ_S, so that it corresponds to the requested steering wheel angle φ_{Srq}. Depending on the steering wheel angle φ_S, the front wheels are ultimately deflected. This results in lateral forces at the front wheels that lead to a change in the lateral motion of the vehicle. The driver perceives this change, so that a corresponding control loop is created in which the driver acts as the controller as well as actuator and sensor. The integration of the driver within this control loop of the lateral motion of the vehicle is shown in Figure 2.4. The modeling of such a driver actuation is described in this chapter.

The resulting DA model consists of a model of the arm muscles and a model of the central nervous system (CNS). The arm muscles perform both actuating and sensory functions: On the one hand, they generate the steering torque T_S as the control variable for controlling the steering wheel angle φ_S and thus the lateral motion of the vehicle. On the other hand, the steering wheel angle φ_S is indirectly sensed by the muscles via the deflection of the muscles and fed back to the CNS, which acts as a controller, using the corresponding sensor signal S_{II} of the muscles. The resulting structure of the DA model, consisting of a CNS model and a muscle model, is shown in Figure 5.3.

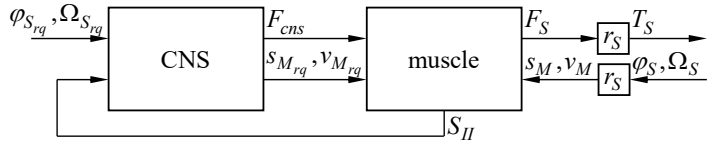

Figure 5.3. Block diagram of the DA model.

The main variables of the DA model are described in Table 5.3. The included muscle model and the CNS model are presented in the following sections.

Table 5.3. Variables of the block diagram of the DA model.

Symbol	Description
F_{cns}	actuating force of the CNS
F_S	muscle force
r_S	steering wheel radius
S_{II}	sensor signal of the approximated muscle deflection
s_M	deflection of the muscle
s_{Mra}	requested deflection of the muscle
T_S	steering torque
v_M	deflection velocity of the muscle
v_{Mra}	requested deflection velocity of the muscle
φ_S	steering wheel angle
φ_{Sra}	requested steering wheel angle
Ω_S	angular velocity of the steering wheel
Ω_{Sra}	requested angular velocity of the steering wheel

5.2.1 Modeling of the Arm Muscles

The arm muscles consist of a combination of extrafusal muscle fibers (eMF) and intrafusal muscle fibers (iMF). A detailed description of the structure of a muscle in terms of its physiology can be found in [59]. An eMF is primarily used to generate the muscle force. In contrast, an iMF contains the muscle sensors for sensing the deflection of the muscle as well as the position error of the muscle deflection. The corresponding sensor signal S_{II} serves as a measure for the deflection of the muscle and thus for the steering wheel angle φ_S via the steering wheel radius r_S. In addition, the sensor signal S_{Ia} of the position error of the muscle deflection is used to generate a reflex force F_{reflex} as an immediate countermeasure to compensate for unexpected disturbances. Figure 5.4 presents the block diagram of the resulting muscle model.

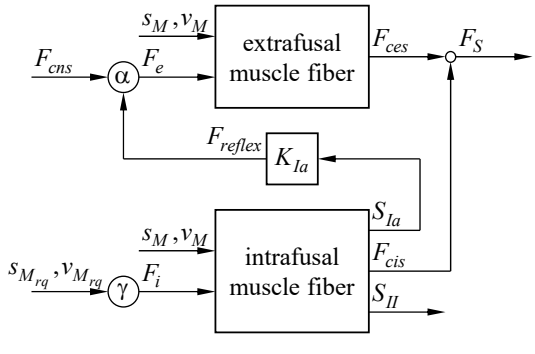

Figure 5.4. Block diagram of the muscle model.

The input variables of the muscle model are the actuating force F_{cns} of the CNS as well as the requested deflection s_{Mrq} and the requested deflection velocity v_{Mrq} of the muscle as output variables of the CNS model. Additionally, the actual deflection s_M and deflection velocity v_M of the muscle are also input variables of the muscle model. These can be determined with the help of the steering wheel radius r_S, based on the steering wheel angle φ_S and the angular velocity Ω_S of the steering wheel as output variables of the SbW model according to Figure 5.3.

The output variable of the muscle model is the muscle force F_S, which in turn is transformed via the steering wheel radius r_S into the steering torque T_S induced at the steering wheel. The muscle force F_S results from the superposition of the forces F_{ces} and F_{cis} generated within the eMF and iMF according to

$$F_S = F_{ces} + F_{cis} \quad . \tag{5.1}$$

The forces F_{ces} and F_{cis} generated within the eMF and iMF represent main variables within the muscle model. Based on the physical substitute model in Figure 5.5, which depicts the basic mechanical characteristics of a muscle, these forces can be described as the spring force of the serial spring of the eMF resp. iMF with the differential equation

$$\frac{b_e}{c_{es}} \dot{F}_{ces} + (1 + \frac{c_{ep}}{c_{es}}) F_{ces} = F_e - b_e v_M - c_{ep} s_M \tag{5.2}$$

and

$$\frac{b_i}{c_{is}} \dot{F}_{cis} + (1 + \frac{c_{ip}}{c_{is}}) F_{cis} = F_i - b_i v_M - c_{ip} s_M \quad . \tag{5.3}$$

Here, b_e and b_i describe the viscous damping constant, and c_{ep} and c_{ip} resp. c_{es} and c_{is} denote the stiffness of the parallel resp. serial spring of the eMF and iMF. [59]

The modeled structure of the two different muscle fibers is identical. Both consist of linear springs and viscous dampers as well as force actuators, as described in [59]. However, the eMF and iMF differ in their parameterization and excitation. For the excitation of the eMF, the α-motoneuron is used,

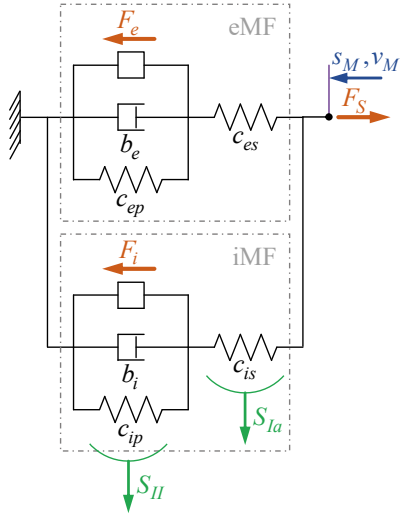

Figure 5.5. Physical substitute model of the muscle.

whereas for the excitation of the iMF, the γ-motoneuron is used (see Figure 5.4). These motoneurons induce the respective actuating forces F_e and F_i. For the actuating force F_e of the eMF, the equation

$$F_e = F_{cns} + F_{reflex} \tag{5.4}$$

follows, with the reflex force

$$F_{reflex} = K_{Ia} S_{Ia} \tag{5.5}$$

as well as the sensor signal S_{Ia} of the position error of the muscle deflection

$$S_{Ia} = a_{aff} \frac{F_{cis}}{c_{is}} \quad , \tag{5.6}$$

which is proportional to the deflection of the serial spring of the iMF. Here, K_{Ia} is a factor for the calculation of the reflex force, while a_{aff} is a factor for the calculation of the afferences. In addition, the actuating force F_i of the iMF can be determined as

$$F_i = b_i v_{M_{rq}} + c_{ip} s_{M_{rq}} \quad . \tag{5.7}$$

Substituting these previous equations into Equation (5.2) and Equation (5.3) yields the final differential equations

$$\frac{b_e}{c_{es}}\dot{F}_{ces} + (1+\frac{c_{ep}}{c_{es}})F_{ces} = F_{cns} + \frac{K_{Ia}a_{ff}}{c_{is}}F_{cis} - b_e v_M - c_{ep}s_M \tag{5.8}$$

and

$$\frac{b_i}{c_{is}}\dot{F}_{cis} + (1+\frac{c_{ip}}{c_{is}})F_{cis} = b_i v_{M_{rq}} - b_i v_M + c_{ip}s_{M_{rq}} - c_{ip}s_M \tag{5.9}$$

for the forces F_{ces} and F_{cis} generated within the eMF and iMF, which produce the resulting muscle force F_S according to Equation (5.1).

Furthermore, the deflection s_M of the muscle is approximated within the iMF and fed back to the CNS in the form of the sensor signal S_{II} based on the deflection of the parallel spring of the iMF. For the sensor signal S_{II} of the approximated muscle deflection, the equation

$$S_{II} = a_{aff}(\frac{F_{cis}}{c_{is}} + s_M) \tag{5.10}$$

results. Together with Equation (5.1) and Equation (5.8) as well as Equation (5.9), Equation (5.10) forms the mathematical model of a muscle. Analyzing these equations shows that the muscle model exhibits PDT2 behavior. This corresponds to the behavior of the muscle spindles formulated in [59]. There, a muscle spindle is described in the medical context as a proportional-differential receptor.

5.2.2 Modeling of the Central Nervous System

In addition to the previously described muscle model, the DA model consists of a suitable model of the CNS as the instance that controls the muscle. The integration of the CNS model within the DA model is shown in Figure 5.3.

The CNS controls the muscle via the actuating force F_{cns} of the CNS, the requested deflection s_{Mrq} and the requested deflection velocity v_{Mrq} of the muscle. With the help of the steering wheel radius r_S, the requested deflection s_{Mrq} and the requested deflection velocity v_{Mrq} of the muscle can be determined from the requested steering wheel angle φ_{Srq} and the requested steering wheel angular velocity Ω_{Srq}, which are input variables of the CNS model. In addition,

the sensor signal S_{II} of the approximated muscle deflection represents a further input variable of the CNS model. Combined with the requested deflection s_{Mrq} of the muscle, an approximate control error of the muscle deflection and thus also of the steering wheel angle can be calculated within the CNS model. In the context of mechatronics, the CNS can therefore be reduced to its function as a steering wheel angle controller, modeled as a PI controller with additional structural measures to improve the control quality. Due to the comparatively large time constants of the muscle model and the SbW model, the latency of the CNS can be neglected.

Choosing a PI controller as a steering wheel angle controller in the CNS model is valid due to the dynamics of the muscle model: The integral part of the PI controller ensures that the resulting steering wheel angle control loop can achieve stationary accuracy. An additional differential part in the CNS model would not provide any benefit: As previously described, the muscle model exhibits PDT2 behavior and therefore already has a differential part. Since an additional differential part in the CNS model would worsen the overall dynamic behavior of the steering wheel angle control loop, it is thus not recommended in the context of modeling the CNS.

The resulting actuating force F_{cns} of the CNS model is the central control variable for generating the muscle force F_S and thus the required steering torque T_S for controlling the steering wheel angle φ_S. Coupling the CNS model with the previously described muscle model yields the DA model.

5.2.3 Modeling of the Steering Angle Control Loop

By controlling the steering wheel angle according to the desired lateral motion of the vehicle, a closed-loop system is created, consisting of the driver and the steering wheel. The steering wheel can be modeled as a simple rotational mass with viscous friction, resulting in the differential equation

$$J_S\dot{\Omega}_S + b_S\Omega_S = T_S - T_{TB} \quad . \tag{5.11}$$

Here, J_S denotes the moment of inertia and b_S the viscous friction of the steering wheel. In addition, the torque T_S describes the input torque of the steering wheel that is equal to the steering torque, while the torque T_{TB} describes the output torque which corresponds to the torsion bar torque in the present SbW system (or the torque at the upper steering column in conventional electromechanical power steering systems).

When this steering model is coupled with the formerly described DA model, a mathematical model of the steering wheel angle control loop is created. This control loop can be used to evaluate the DA model.

5.2.4 Evaluation of the Driver Actuation Model

To evaluate the derived DA model, the parameters of the model are first identified. For this, tests are performed on a driving simulator that emulates the real environment of the steering wheel angle control loop. The driving simulator consists of a physical representation of the FU including an inverter and a connected real-time system with a HMI. Figure 5.6 depicts the schematic structure of the driving simulator. The FU combines a steering wheel and a feedback actuator, which can realize desired time histories for the torsion bar torque T_{TB} as input variable of the steering angle control loop, allowing the stimulation of the steering wheel angle control loop to identify the parameters of the DA model as described in [60]-[63]. The result is an optimally identified and parameterized DA model. Figure 5.7 shows a picture of the driving simulator.

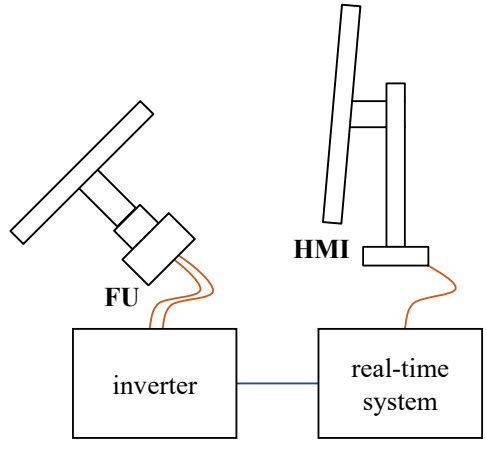

Figure 5.6. Schematic structure of the driving simulator.

For practical implementation, a DA model of the lowest possible order is desired. Therefore, a reduced model is derived from the detailed model resp. the results of the system identification. This reduced DA model replicates all dominant characteristics of a real driver. It corresponds to a spring-damper element combined with a first order lag system, described by the differential equation

$$\dot{x}_{DA} = -\frac{1}{\tau_{DA}} x_{DA} + \frac{1}{\tau_{DA}} \varphi_{S_{rq}} \tag{5.12}$$

and the algebraic equation

$$T_S = -\frac{b_{DA}}{\tau_{DA}} x_{DA} + (c_{DA} + \frac{b_{DA}}{\tau_{DA}})\varphi_{S_{rq}} - c_{DA}\varphi_S - b_{DA}\Omega_S \tag{5.13}$$

with the requested steering wheel angle φ_{Srq} as well as the actual steering wheel angle φ_S and the steering wheel angular velocity Ω_S as input variables and the steering torque T_S as the output variable. In addition, x_{DA} denotes the state variable of the reduced model. Furthermore, c_{DA} describes the stiffness and b_{DA} the viscous damping constant of the spring-damper element as well as τ_{DA} the time constant of the first order lag system.

Figure 5.7. Picture of the driving simulator.

Combining the steering model from Equation (5.11) with the DA model from Equation (5.12) and Equation (5.13) yields the state-space representation

$$\begin{aligned} \dot{\underline{x}}_{SC}(t) &= \underline{A}_{SC}\underline{x}_{SC}(t) + \underline{B}_{SC}\underline{u}_{SC}(t) \;\;,\;\; \underline{x}_{SC}(0) = \underline{x}_{SC,0} \\ \underline{y}_{SC}(t) &= \underline{C}_{SC}\underline{x}_{SC}(t) + \underline{D}_{SC}\underline{u}_{SC}(t) \end{aligned} \tag{5.14}$$

of the model for the steering angle control loop with the state-space matrices

$$\underline{A}_{SC} = \begin{bmatrix} 0 & 1 & 0 \\ -\frac{c_{DA}}{J_S} & -\frac{b_S + b_{DA}}{J_S} & -\frac{b_{DA}}{J_S \tau_{DA}} \\ 0 & 0 & -\frac{1}{\tau_{DA}} \end{bmatrix} , \tag{5.15}$$

$$\underline{B}_{SC} = \begin{bmatrix} 0 & 0 \\ \dfrac{c_{DA}}{J_S} + \dfrac{b_{DA}}{J_S \tau_{DA}} & -\dfrac{1}{J_S} \\ \dfrac{1}{\tau_{DA}} & 0 \end{bmatrix}, \tag{5.16}$$

$$\underline{C}_{SC} = \begin{bmatrix} 1 & 0 & 0 \\ -c_{DA} & -b_{DA} & -\dfrac{b_{DA}}{\tau_{DA}} \end{bmatrix}, \tag{5.17}$$

$$\underline{D}_{SC} = \begin{bmatrix} 0 & 0 \\ c_{DA} + \dfrac{b_{DA}}{\tau_{DA}} & 0 \end{bmatrix} \tag{5.18}$$

and the state, input and output vector

$$\underline{x}_{SC}(t) = \begin{bmatrix} \varphi_S(t) \\ \Omega_S(t) \\ x_{DA}(t) \end{bmatrix}, \ \underline{u}_{SC}(t) = \begin{bmatrix} \varphi_{S_{rq}}(t) \\ T_{TB}(t) \end{bmatrix}, \ \underline{y}_{SC}(t) = \begin{bmatrix} \varphi_S(t) \\ T_S(t) \end{bmatrix}. \tag{5.19}$$

The input variables for the model are the requested steering wheel angle φ_{Srq} as well as the torsion bar torque T_{TB}, whereas the output variables are the resulting steering wheel angle φ_S as well as the steering torque T_S induced at the steering wheel by the DA model.

This model for the steering angle control loop is subsequently employed to evaluate the performance of the derived DA model. For this, the model for the steering angle control loop is coupled with the control algorithm from Chapter 4, the detailed AU model from Chapter 3.1 and the VD model from Chapter 5.1, so that a representative FU motor torque is generated for a defined driving situation. This augmented model forms the simulation model with which the same experiments are performed as with the driving simulator. To ensure that the simulated and measured results can be compared, the driving simulator is also coupled to the same models. The block diagram of the resulting driving simulator is illustrated in Figure 5.8.

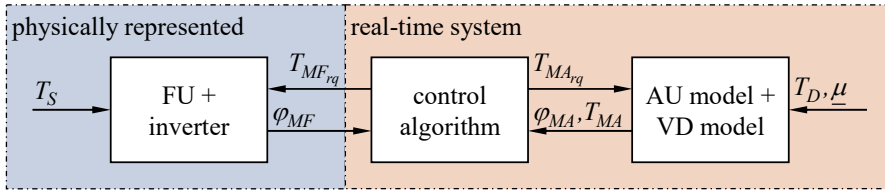

Figure 5.8. Block diagram of the driving simulator.

Exemplary results of the conducted experiments are described in the following sections. There, the identified parameterization of the DA model according to Table 5.4 is used.

Table 5.4. Exemplary parameters of the reduced DA model.

Symbol	Description	Value
c_{DA}	stiffness	115 Nm/rad
b_{DA}	damping constant	8 Nms/rad
τ_{DA}	time constant	1 ms

5.2.4.1 Step Response

In the first experiment, the step response of the steering angle control loop is analyzed. The requested steering wheel angle φ_{Srq} as input of the DA model is step-shaped increased from 0 rad to π/2 rad (90°) at 1 s, while maintaining a low vehicle velocity v_V of 10 km/h. This results in an actual steering wheel angle φ_S and, depending on the driving maneuver, a torsion bar torque T_{TB} that counteracts the steering torque T_S. The corresponding simulated time histories of the steering wheel angle φ_S and the steering torque T_S are shown in Figure 5.9. The measured time histories, realized by a real driver interacting with the steering wheel of the driving simulator, are also displayed in Figure 5.9.

The results demonstrate a strong correlation between the simulated and measured data throughout the entire experiment. This indicates that the derived DA model accurately replicates real driver behavior. This is also observed in the following experiments.

5.2.4.2 Fishhook

The experiments performed to evaluate the derived DA model shall include critical driving maneuvers. Therefore, a variation of the fishhook road test is conducted as a second experiment. The fishhook road test is a common road test with highly dynamic excitations to test the rollover propensity of a vehicle in a severe change of the driving direction. Detailed description of this test procedure can be found in [64][65].

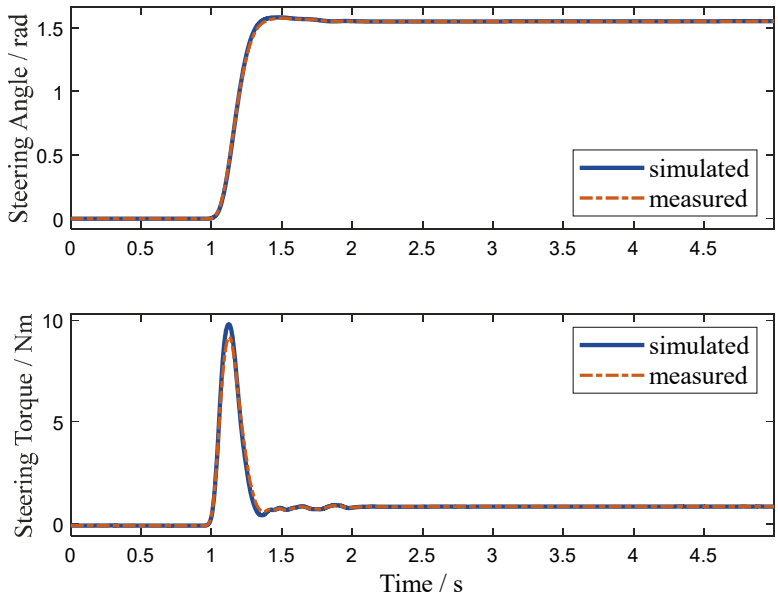

Figure 5.9. Time histories of the simulated and measured steering wheel angle φ_S (top) and steering torque T_S (bottom) for step-shaped excitation.

The fishhook road test is characterized by two rapid changes of the requested steering wheel angle φ_{Srq} (resp. the actual steering wheel angle φ_S) to nearly -π /2 rad (-90°) resp. π/2 rad (90°) at the beginning of the test. Both changes have a high gradient up to 4π rad/s (720°/s). Here, the vehicle velocity v_V is 50 km/h. The corresponding simulated and measured time histories of the steering wheel angle φ_S and the steering torque T_S are shown in Figure 5.10.

Consistent with the previously shown experiment, the simulated and the measured results closely align throughout this experiment, confirming the accuracy and reliability of the derived DA model.

5.2.4.3 Multiple Lane Change

In the third experiment, a multiple lane change is analyzed as another experiment with highly dynamic excitations. The vehicle velocity v_V is held constant at 70 km/h. The corresponding simulated and measured time histories of the steering wheel angle φ_S and the steering torque T_S are depicted in Figure 5.11.

As before, it can be seen that both the time history of the steering wheel angle φ_S as well as the time history of the steering torque T_S of the simulation and the measurement are nearly identical. Further experiments were performed that resulted in the same conclusion. The derived DA model can therefore be considered optimal both in terms of its structure and its parameterization.

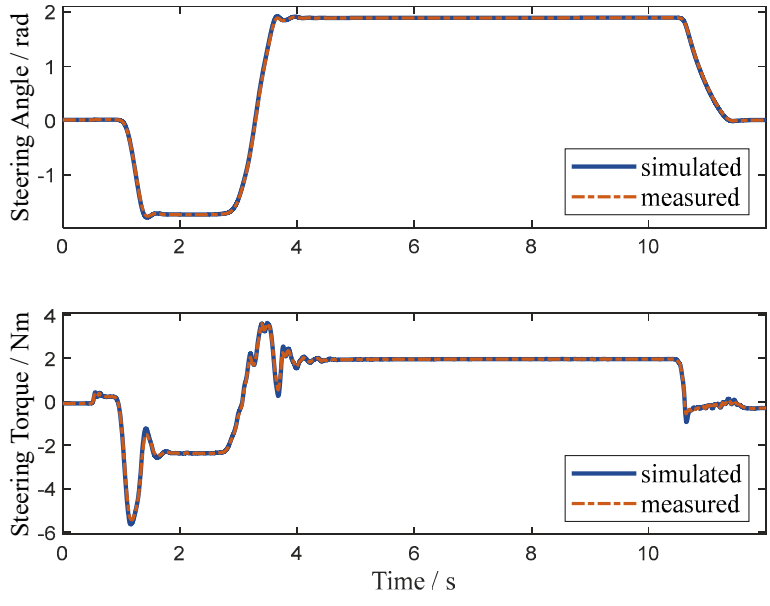

Figure 5.10. Time histories of the simulated and measured steering wheel angle φ_S (top) and steering torque T_S (bottom) for fishhook.

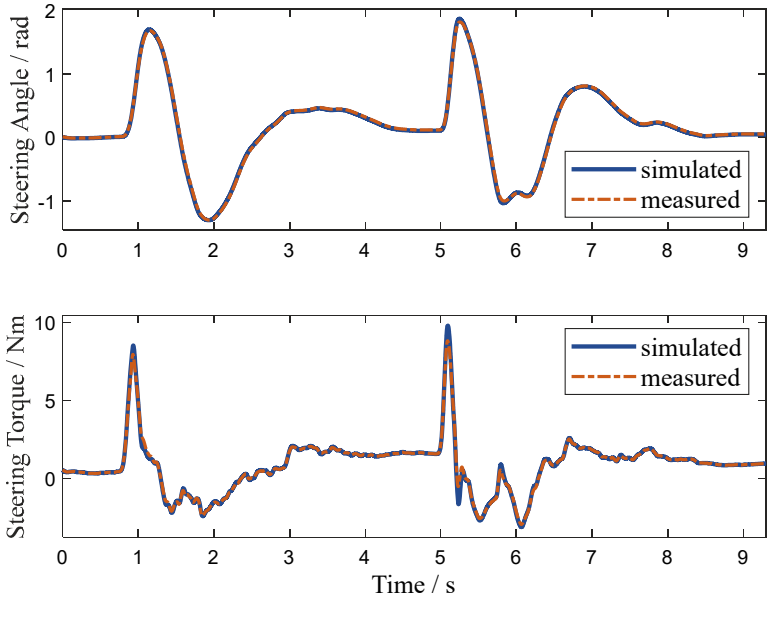

Figure 5.11. Time histories of the simulated and measured steering wheel angle φ_S (top) and steering torque T_S (bottom) for multiple lane change.

5.3 Simulation Results

Now that the models of the augmented simulation environment for the developed control algorithm have been derived in the previous sections, the corresponding discrete augmented control system resulting from Figure 5.1 can be analyzed. Figure 5.12 and Figure 5.13 illustrate the step responses of the discrete augmented control system from a requested steering wheel angle φ_{Srq} to the two controlled variables s_R and T_{TB}.

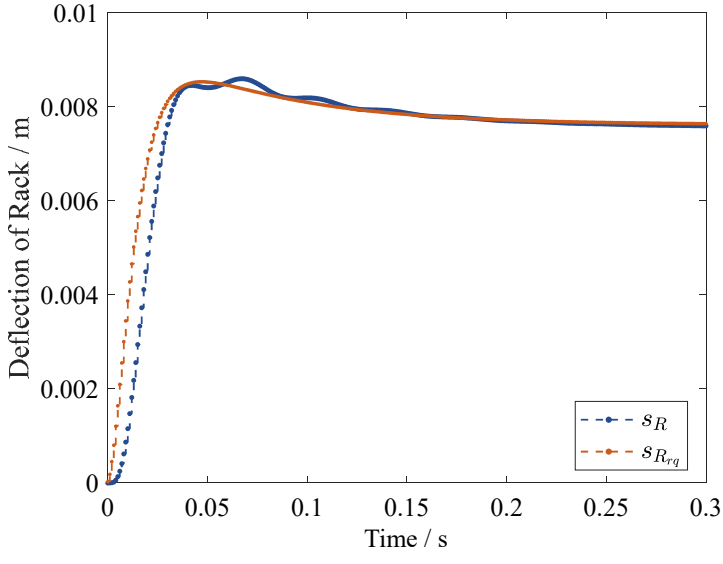

Figure 5.12. Step response of the discrete augmented control system from the requested steering wheel angle φ_{Srq} to the deflection s_R of the rack (blue) and the requested deflection s_{Rrq} of the rack (orange).

The driver's steering request results in a rapid increase of the steering wheel angle φ_S and thus to a corresponding requested deflection s_{Rrq} of the rack of over 8.5 mm in less than 50 ms. The magnitude of the requested deflection s_{Rrq} depends on the virtual gear ratio parameterized in the position generator from Chapter 4.2. The discrete LQG compensator adjusts the actual deflection s_R of the rack to the requested deflection s_{Rrq}, yielding the time histories shown in Figure 5.12. It is evident that the discrete LQG compensator can realize such highly dynamic steering requests. Simultaneously, the system response is sufficiently damped, despite the large number of viscoelastic elements within the detailed SbW model. Thus, the actual deflection s_R of the rack remains within a tolerance band of ±5 % around the requested deflection s_{Rrq} after approximately 30 ms. Additionally, no significant overshoot is observable. In this way, the control also ensures that the requirements for autonomous

driving are fulfilled, as it enables the instantaneous and robust control of the lateral motion of a vehicle.

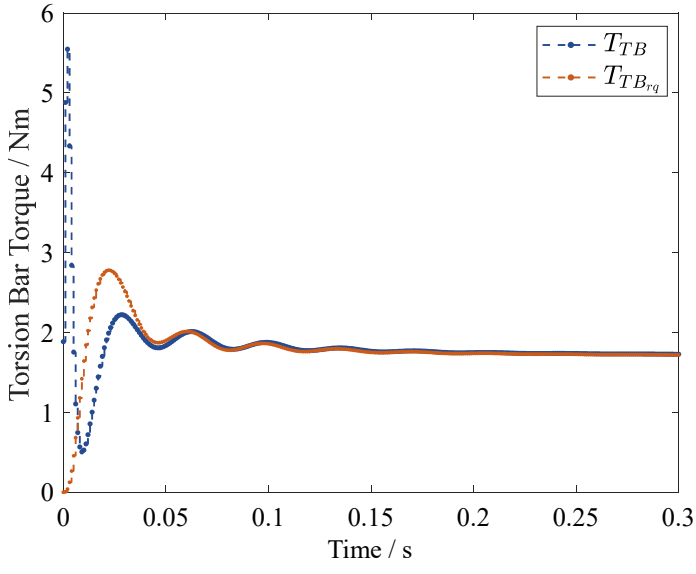

Figure 5.13. Step response of the discrete augmented control system from the requested steering wheel angle $\varphi_{S_{rq}}$ to the torsion bar torque T_{TB} (blue) and the requested torsion bar torque $T_{TB_{rq}}$ (orange).

A deflection s_R of the rack resp. the wheels causes a change of the torques T_{WL} and T_{WR} about the steering axis of the left and right front wheel and thus a change of the equivalent rack force F_R. This leads to a requested torsion bar torque T_{TBrq}, which should provide the driver with feedback on the current driving situation. The magnitude of the requested torsion bar torque T_{TBrq} depends on the parametrization of the feeling generator. The discrete LQG compensator then adjusts the actual torsion bar torque T_{TB} to the requested torque T_{TBrq}, yielding the time histories shown in Figure 5.13. Due to the highly dynamic characteristic of the steering request, the DA model initially generates a high steering torque T_S, resulting in a significant torsion bar torque T_{TB}. However, the discrete LQG compensator quickly compensates this and adjusts the actual torsion bar torque T_{TB} to the requested torsion bar torque T_{TBrq}, ensuring that the driver promptly experiences the desired feedback. Consequently, the actual torsion bar torque T_{TB} remains within a tolerance band of ±5 % around the requested torque T_{TBrq} after about 40 ms. Moreover, there is no significant overshoot.

It is evident that the control system fulfills the requirements specified at the beginning of this chapter. Thus, the developed control approach ensures good

characteristics and answers the second research question from Chapter 1.1. [1] Further results of the conducted analysis of the control system are documented in Paper II and Paper III. In the following chapter, the good characteristics of the control approach ensured in the simulation are further validated on a test bench.

6 Realization and Experimental Study

The final steps of the MDC are the realization of the developed control algorithm and conducting experiments with a real prototype to validate the control algorithm in a real-world environment. This chapter provides a description of the corresponding process steps.

6.1 Method

The realization of the control is the fifth step of the MDC. In this step, a test bench is built as a prototype of the mechatronic system. The mechanical and electrical components are designed, manufactured and assembled. Additionally, the signal processing components are programmed and implemented on suitable high-performance hardware. Figure 6.1 illustrates the individual process steps from the control system to a test bench for validating the control in a real-world environment.

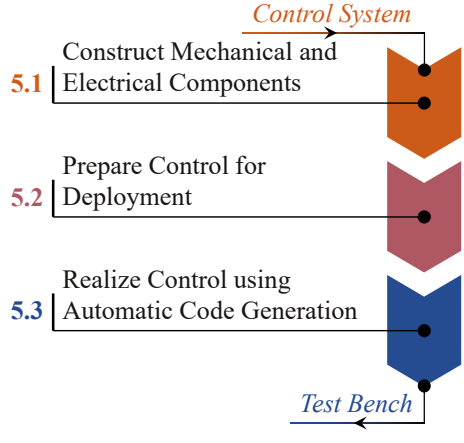

Figure 6.1. Process steps of the realization.

In preparation for deployment, the previously designed control algorithm is extracted from the simulation environment. The input and output channels of the development hardware are defined and extensions required for real-time

operation are made. Subsequently, the control algorithm is implemented using automatic code generation within the development environment. A coder translates the control algorithm into C code, augmenting the code with a real-time core controlled by a timer interrupt, input and output functions, initialization code for the interfaces and more. The resulting real-time code is then compiled, linked and loaded onto the test bench hardware. [8][64] Afterwards, the control algorithm can be operated and tested on the test bench. Here, the driving simulator from Figure 5.8 is used as the test bench.

6.2 Measurement Results

The experimental study represents the final step of the MDC. In this step, the same experiments are conducted on the real test bench as in the simulation (see Chapter 5). If the characteristics from the measurement correspond to the characteristics from the simulation, the MDC ends with an optimal prototype. Conversely, if deviations are observed, previous steps of the MDC must be reviewed and optimized. Figure 6.2 shows the individual process steps of the experimental study.

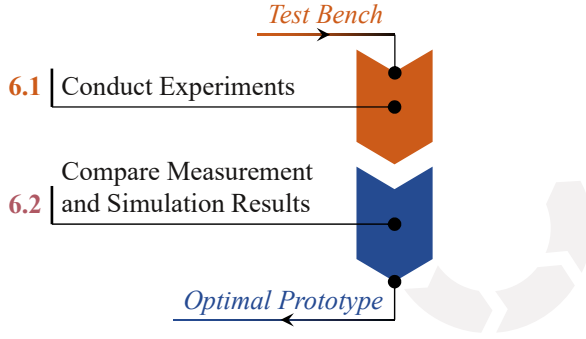

Figure 6.2. Process steps of the experimental study.

6.2.1 Step Response

In the first experiment, the step response is analyzed again. For this, a driver adjusts the steering wheel angle φ_S on the driving simulator to follow a requested steering wheel angle φ_{Srq} that is step-shaped increased from 0 rad to $\pi/2$ rad (90°) at 1 s, while maintaining a low vehicle velocity v_V of 10 km/h. The driver accomplishes this by applying a steering torque T_S at the steering wheel, which causes a change in the steering wheel angle φ_S. Based on the

steering wheel angle φ_S, a requested AU motor angle φ_{MArq} is generated, resulting in a corresponding actual AU motor angle φ_{MA} and thus a deflection s_R of the rack. This, in turn, ultimately results in a steering angle φ_{WL} and φ_{WR} of the left and right front wheel according to the driver's intentions[8]. Consequently, depending on the current driving situation, forces and torques act on the front wheels due to the road contact, which can be transformed into an equivalent rack force F_R. To provide the driver with feedback on the current driving situation, the rack force F_R leads to a corresponding requested torsion bar torque T_{TBrq}. The time histories of the measured steering torque T_S, steering wheel angle φ_S, requested and actual AU motor angle φ_{MArq} and φ_{MA} as well as the requested and actual steering torque T_{TBrq} and T_{TB} are depicted in Figure 6.3 for this experiment. The resulting rack force F_R, along with the requested and actual AU motor torque T_{MArq} and T_{MA} as well as the requested and actual FU motor torque T_{MFrq} and T_{MF}, are displayed in Figure 6.4.

The controlled variables φ_{MA} and T_{TB} follow the reference variables φ_{MArq} and T_{TBrq} immediately. In addition, there are no large overshoots and no steady-state control errors. Moreover, the amplitudes of the control variables T_{MArq} and T_{MFrq} are sufficient small, ensuring minimal energy consumption while maintaining high control quality. Furthermore, the measurement on the test bench verifies the results of the simulation. For a comparison between simulation and measurement, see Chapter 5.2.4.1.

6.2.2 Multiple Steering

In the second experiment, multiple steering maneuvers are performed at a medium vehicle velocity v_V of 50 km/h. Initially, the driver deflects the steering wheel by π rad (180°) at 1 s. The steering wheel angle φ_S is then held constant until the driver releases the steering wheel at 3 s. The centering component in the control algorithm ensures that the steering wheel is returned smoothly to its center position so that the vehicle drives in a straight line by 5 s. This steering maneuver is repeated in the negative direction at 12 s. Additionally, the steering wheel is deflected again in the positive direction by π rad (180°) at 23 s. This time, however, the driver does not release the steering wheel, but actively steers the steering wheel back to a negative steering wheel angle φ_S of -π rad (-180°) and then returns it back to its center position. The resulting time history of the steering wheel angle φ_S and the associated time history of

[8] The deflection s_R of the rack was not available as a measured variable on the test bench. As a substitute, the AU motor angle φ_{MA} is compared here and in the following with the corresponding requested AU motor angle φ_{MArq}.

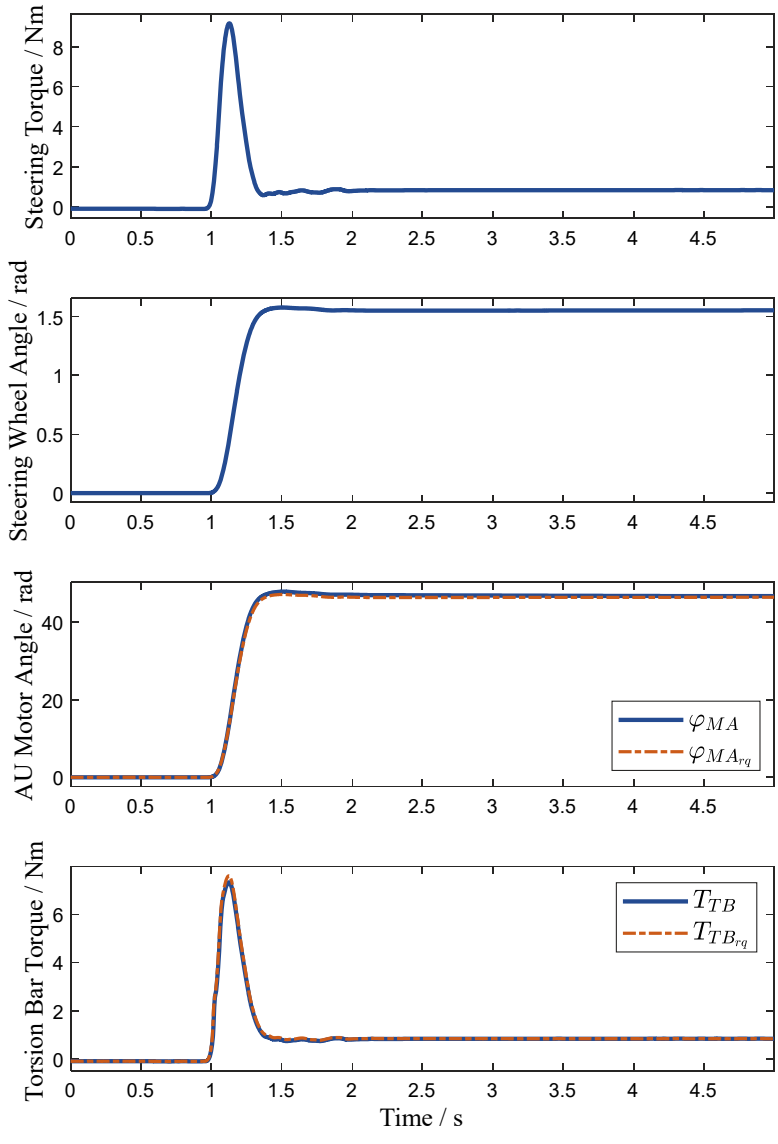

Figure 6.3. Time histories of the measured steering torque T_S (top), steering wheel angle φ_S (second), AU motor angle φ_{MA} (third, blue) and corresponding requested AU motor angle φ_{MArq} (third, orange) as well as torsion bar torque T_{TB} (bottom, blue) and corresponding requested torsion bar torque T_{TBrq} (bottom, orange) for step-shaped excitation.

the steering torque T_S are depicted in Figure 6.5. This figure also shows the time histories of the two controlled variables φ_{MA} and T_{TB}, alongside their corresponding reference variables φ_{MArq} and T_{TBrq}. As in the previous experiment, the controlled variables φ_{MA} and T_{TB} closely follow the reference variables φ_{MArq} and T_{TBrq}.

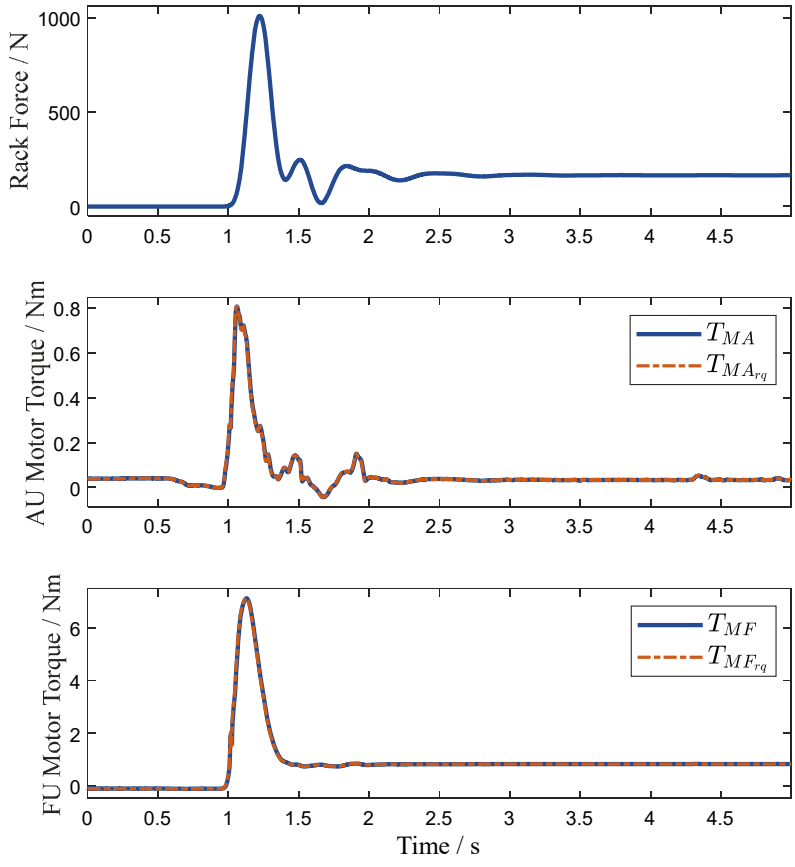

Figure 6.4. Time histories of the measured rack force F_R (top), AU motor torque T_{MA} (center, blue) and corresponding requested AU motor torque T_{MArq} (center, orange) as well as FU motor torque T_{MF} (bottom, blue) and corresponding requested FU motor torque T_{MFrq} (bottom, orange) for step-shaped excitation.

Furthermore, the control algorithm detects when the driver releases the steering wheel (see vertical gray dashed lines in Figure 6.5), which is indicated by a decrease of the steering torque T_S to 0 Nm. Consequently, an appropriate requested torsion bar torque T_{TBrq} is generated to return the steering wheel back to its center position at a desired angular velocity of the steering wheel. The peaks that then occur in the requested torsion bar torque T_{TBrq} are caused by the control algorithm, compensating for the static friction of the steering wheel to steer it to the exact center position.

The resulting torsion bar torque T_{TB} also influences the measurement resp. estimate of the steering torque T_S, resulting in an increased noise amplitude over the corresponding time period. As the steering wheel is steered back to

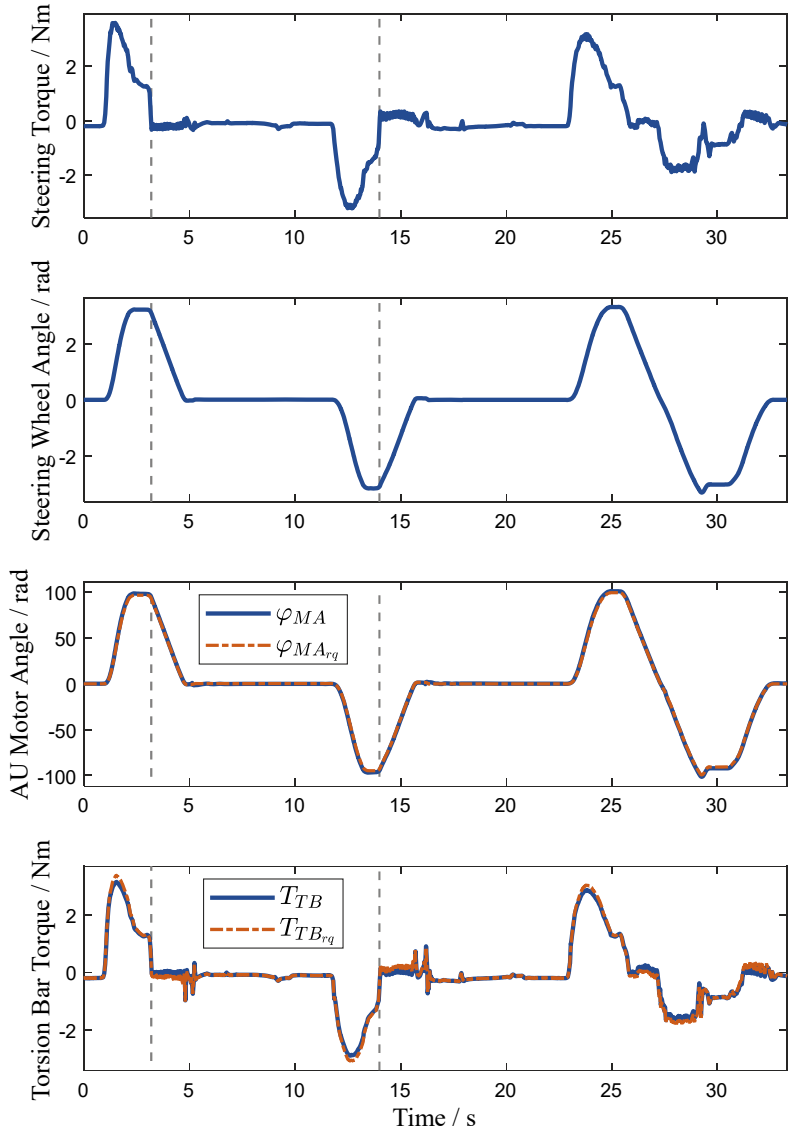

Figure 6.5. Time histories of the measured steering torque T_S (top), steering wheel angle φ_S (second), AU motor angle φ_{MA} (third, blue) and corresponding requested AU motor angle φ_{MArq} (third, orange) as well as torsion bar torque T_{TB} (bottom, blue) and corresponding requested torsion bar torque T_{TBrq} (bottom, orange) for multiple steering.

its center position, the front wheels of the vehicle are simultaneously turned back to their center position by the AU motor so that the driver's intentions are followed smoothly throughout the entire experiment.

6.2.3 Fishhook

The third experiment presented is the fishhook road test with its highly dynamic excitations at a medium vehicle velocity v_V of 50 km/h. Initially, the steering wheel is deflected to -1.7 rad (-100°). The steering wheel angle φ_S is then held constant for about one second before the steering wheel is deflected to 1.9 rad (110°) and held in this position for about seven seconds. Finally, the steering wheel is returned to its center position at the end of the experiment. The resulting time histories of the measured steering torque T_S, steering wheel angle φ_S, requested and actual AU motor angle φ_{MArq} and φ_{MA} as well as the requested and actual steering torque T_{TBrq} and T_{TB} are shown in Figure 6.6.

Despite the highly dynamic excitation, the controlled variables φ_{MA} and T_{TB} follow the reference variables φ_{MArq} and T_{TBrq} well. Moreover, the measurement on the test bench verifies the simulation results. For a comparison between simulation and measurement, see Chapter 5.2.4.2.

6.2.4 Double Lane Change

The fourth experiment involves a double lane change at a high vehicle velocity v_V of 70 km/h. The double lane change is a road test that is used to evaluate the behavior of a vehicle in an obstacle avoidance maneuver. Hence, it is also suitable to evaluate the performance of the developed control algorithm. The resulting time histories of the measured steering torque T_S, steering wheel angle φ_S, requested and actual AU motor angle φ_{MArq} and φ_{MA} as well as the requested and actual steering torque T_{TBrq} and T_{TB} are depicted in Figure 6.7. The test procedure of the double lane change is documented in detail in [64]0.

In accordance with the previous experiments, the controlled variables φ_{MA} and T_{TB} closely follow the reference variables φ_{MArq} and T_{TBrq}.

6.2.5 Free Drive

As the final experiment, a free drive at a vehicle velocity v_V of 30 km/h is shown to verify the performance of the control algorithm in typical driving situations. This driving maneuver includes a gentle left-hand bend, followed by a left turn and a diagonal drive over a speed bump. The resulting time histories of the measured steering torque T_S, steering wheel angle φ_S, requested and actual AU motor angle φ_{MArq} and φ_{MA} as well as the requested and actual steering torque T_{TBrq} and T_{TB} are displayed in Figure 6.8. Additionally, the corresponding rack force F_R, requested and actual AU motor torque T_{MArq} and T_{MA} as well as the requested and actual FU motor torque T_{MFrq} and T_{MF} are visualized in Figure 6.9.

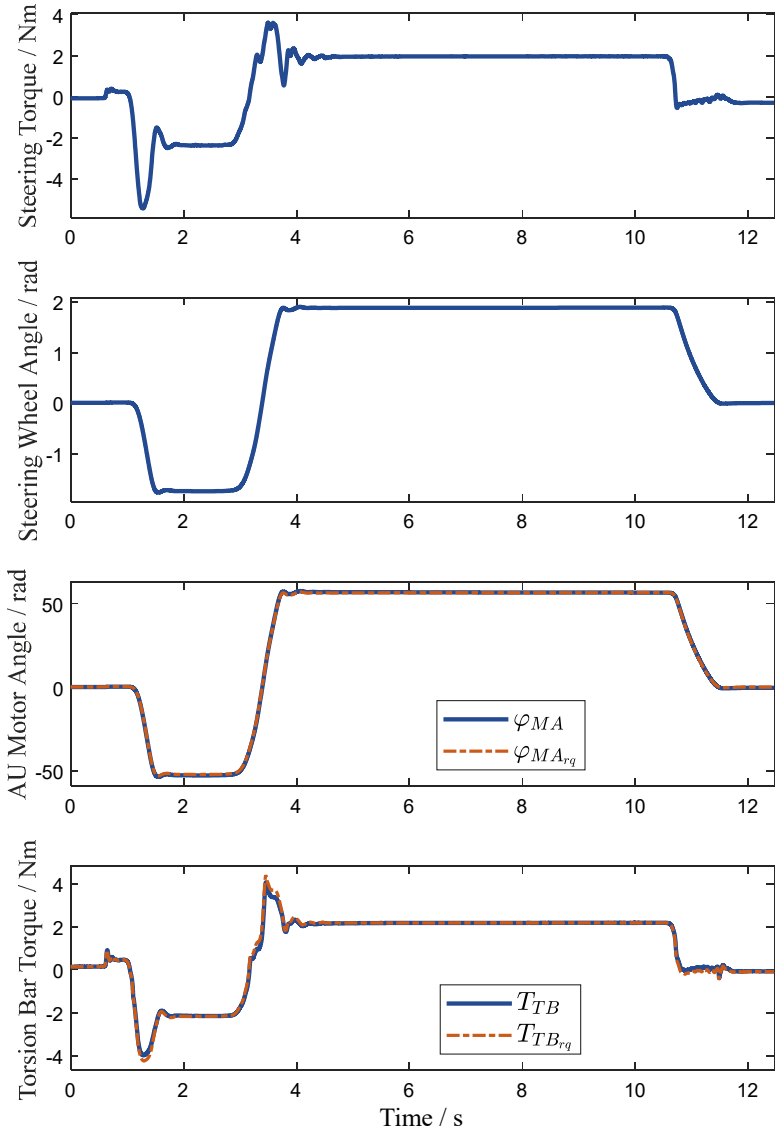

Figure 6.6. Time histories of the measured steering torque T_S (top), steering wheel angle φ_S (second), AU motor angle φ_{MA} (third, blue) and corresponding requested AU motor angle φ_{MArq} (third, orange) as well as torsion bar torque T_{TB} (bottom, blue) and corresponding requested torsion bar torque T_{TBrq} (bottom, orange) for fishhook.

The impact of driving over the speed bump can be observed in Figure 6.9 by the large amplitudes at 78 s. In Figure 6.8, the drive over the speed bump is indicated by the vertical gray dashed lines.

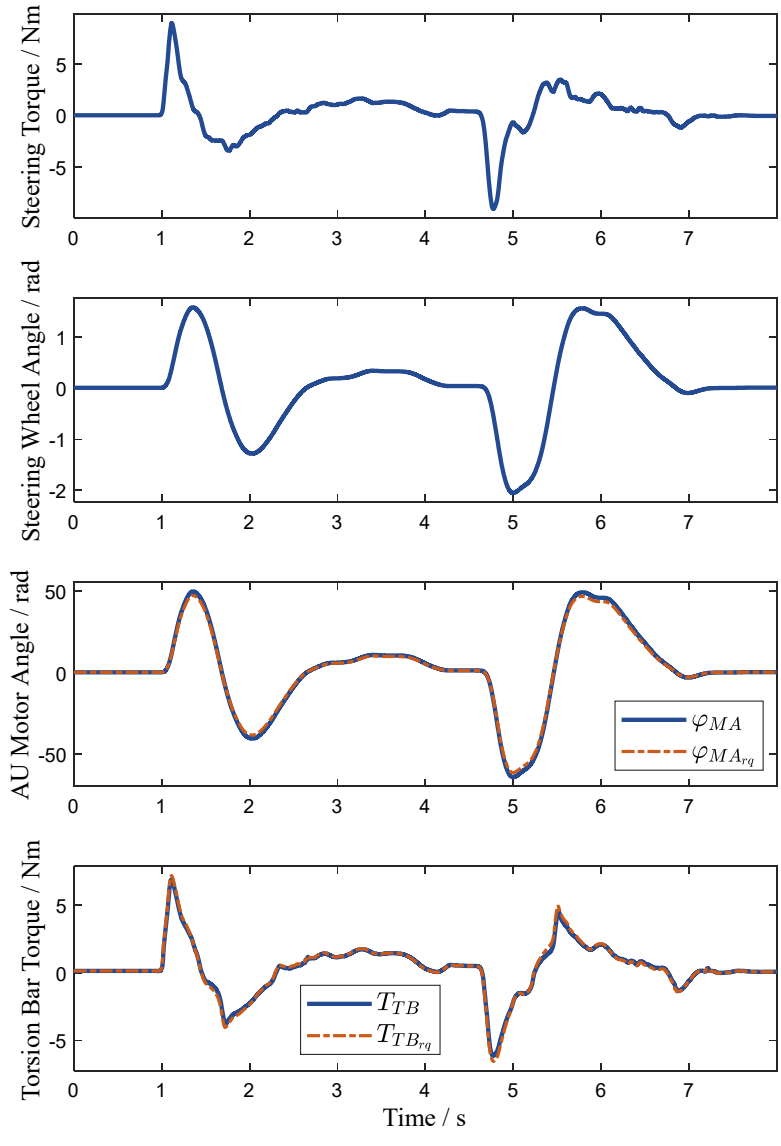

Figure 6.7. Time histories of the measured steering torque T_S (top), steering wheel angle φ_S (second), AU motor angle φ_{MA} (third, blue) and corresponding requested AU motor angle φ_{MArq} (third, orange) as well as torsion bar torque T_{TB} (bottom, blue) and corresponding requested torsion bar torque T_{TBrq} (bottom, orange) for double lane change.

The time history of the torsion bar torque T_{TB} and the steering torque T_S show that the impact of the speed bump is fed back to the driver as desired. Nevertheless, the effect of the speed bump on the lateral motion of the vehicle is compensated by the control algorithm, as can be seen from the smooth gradient of the steering wheel angle φ_S and the AU motor angle φ_{MA}.

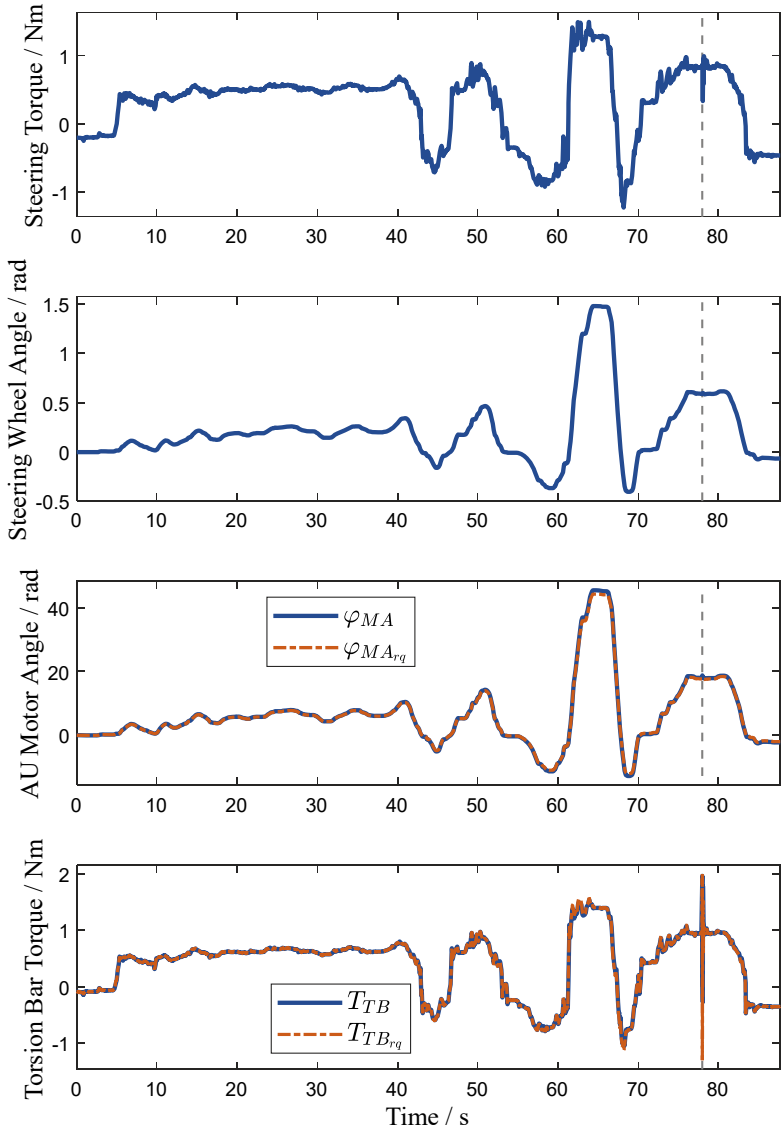

Figure 6.8. Time histories of the measured steering torque T_S (top), steering wheel angle φ_S (second), AU motor angle φ_{MA} (third, blue) and corresponding requested AU motor angle φ_{MArq} (third, orange) as well as torsion bar torque T_{TB} (bottom, blue) and corresponding requested torsion bar torque T_{TBrq} (bottom, orange) for free drive.

In this final experiment, the controlled variables φ_{MA} and T_{TB} also follow the reference variables φ_{MArq} and T_{TBrq} precisely. Further experiments were performed which yielded the same conclusion. Therefore, the experiments confirm that the good characteristics of the control algorithm determined in the

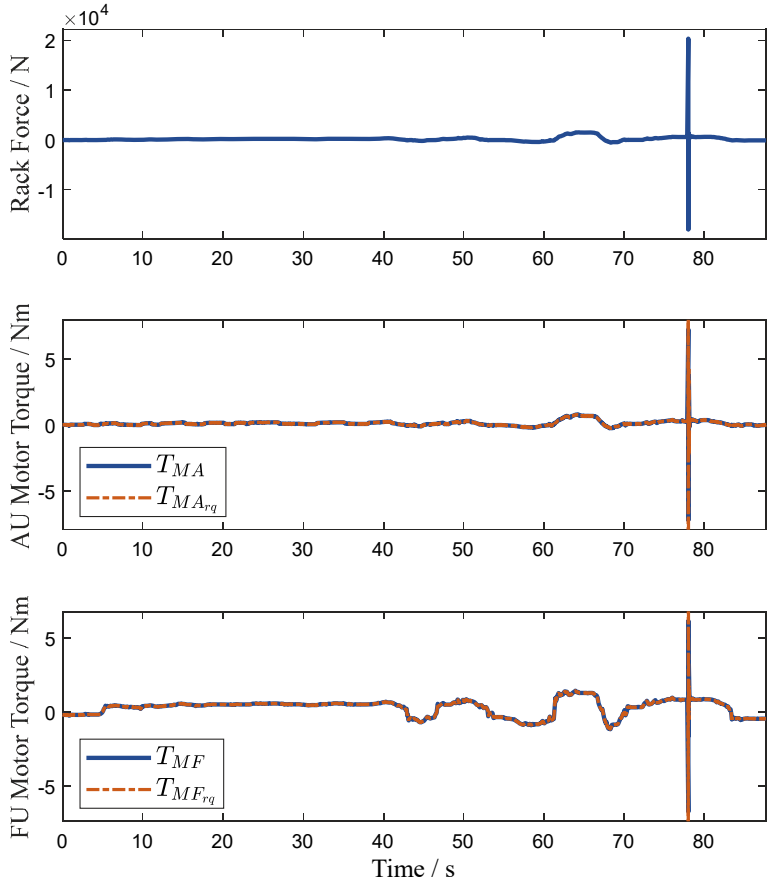

Figure 6.9. Time histories of the measured rack force F_R (top), AU motor torque T_{MA} (center, blue) and corresponding requested AU motor torque T_{MArq} (center, orange) as well as FU motor torque T_{MF} (bottom, blue) and corresponding requested FU motor torque T_{MFrq} (bottom, orange) for free drive.

simulation are also valid in the real environment, so that the MDC from Figure 1.2 can be concluded with an optimal prototype. Thus, the third and final research question outlined in Chapter 1.1 is optimally answered.

7 Summary and Conclusion

The following chapter is adapted from the author's licentiate thesis [1].

The development of autonomous driving systems requires advanced control approaches, simulation methods and agile development strategies. Consequently, this dissertation addressed the author's research in the development and simulation of innovative technologies and control systems to improve the performance and sustainability of vehicles. The associated papers cover various approaches for optimizing vehicle systems and processes in the automotive industry. Particular emphasis was placed on the model-based design, control engineering, virtual testing and optimization of steering systems. Modern Steer-by-Wire systems represent a key technology in this context, as they are crucial for the advancement of highly automated and autonomous vehicles. This led to the following primary research question of this dissertation:

How can highly dynamic control approaches for modern Steer-by-Wire systems be designed, which simultaneously guarantee an extremely high robustness?

To answer this question, the mechatronic development cycle was utilized to improve the robustness of Steer-by-Wire systems through an optimal model-based design of a novel multivariable control approach. This approach significantly increases the robustness of the resulting control system and its performance under varying driving conditions, compared to traditional single-input single-output control designs.

The development required optimal models that accurately reflect the dominant characteristics of a real Steer-by-Wire system (Paper I), which led to the first more specific research question of how to obtain a minimal and **optimal level of detail for modeling** the characteristics of a Steer-by-Wire system. To answer this question, a detailed model was developed that represents all characteristics of a real Steer-by-Wire system. Based on a comprehensive dominance analysis of this detailed model, a reduced optimal model was derived. The corresponding modeling and model analysis provided profound insight into a Steer-by-Wire system and enabled the design of a highly robust steering

control. For the control design, the entire environment in which a Steer-by-Wire system operates was considered, including the feeling generator that determines the desired steering feel for the current driving situation (Paper II and Paper III).

This led to the second specific research question of how the corresponding control algorithm can be **comprehensively virtually tested** in the simulation. To answer this question, an augmented simulation environment was developed that can simulate the real environment of a Steer-by-Wire system and thus real driving maneuvers. The control algorithm was afterwards extensively analyzed within this augmented simulation environment, to ensure that the control algorithm met all specified requirements. The development of this realistic simulation environment enabled the assessment of the system behavior in real-world scenarios, thus validating the effectiveness of the proposed control algorithm. For this purpose, a vehicle dynamics model with multivariable control was developed (Paper IV). The knowledge gained from the development of the corresponding multibody models and optimal control was also applied to large-volume and heavy-duty transports as well as light electric vehicles. For instance, a vehicle dynamics model with a variable number of trailers was developed, which facilitated the design of an enhanced methodology for the three-dimensional trafficability analysis with collision detection of a transport (Paper V). As another example, the model-based development of a cargo bike was carried out and a prototype for data collection was built, thus allowing the verification of the fundamental vehicle dynamics model (Paper VI). The data collected can also be used to develop additional models and driver assistance systems within the simulation. Furthermore, the simulation environment supports not only the development of Steer-by-Wire systems and the analysis of automated driving functions, but also the evaluation of sensor and perception systems (Paper IX, Paper X and Paper XIV). Consequently, virtual testing enabled realistic investigation of vehicle behavior and traffic interactions (Paper VII and Paper VIII).

In addition, the simulation environment also helped to answer the final specific research question of how to migrate experiments that are currently being conducted with test vehicles to a **test bench** in order to obtain an **optimal prototype** at an early stage of development. For this purpose, the test bench was built using the previously developed models, allowing the control algorithm to be validated in a real-world environment and thus emphasizing its real-world applicability (Paper VI). The results demonstrate not only the feasibility but also the advantages of implementing the derived control algorithm in Steer-by-Wire systems, thereby contributing to the broader field of mechatronic and automotive innovation. These developments lead to an increased

efficiency and process optimization in the automotive industry. This is exemplified in the development of predictive models, intelligent analysis methods and the utilization of AI for forecasting (Paper XI, Paper XII, Paper XIII and Paper XV).

The related papers illustrate the development of new technologies and control systems to improve the safety, efficiency and innovation of vehicles. Control engineering, driver assistance systems, virtual testing and process optimization are key areas of current research for advancing the automotive industry. The common aspects of the papers highlight the interdisciplinary nature of the research and the need for collaboration to create forward-looking solutions. Hence, the author's research advances autonomous driving technologies through model-based design, robust control, virtual testing, integration of human interaction and uncertainty management. This multidisciplinary approach enables multi-objective optimization at an early stage of product development, allowing for parameter variations based on circular economy requirements. Additionally, it minimizes time- and cost-intensive testing on prototypes, avoids unnecessary iterations in the design and significantly increases the efficiency and quality of the development. Moreover, it is essential for developing novel autonomous driving systems in modern vehicles.

In conclusion, this dissertation provides valuable insights and approaches for enhancing the design and control of Steer-by-Wire systems. Future research could extend these strategies to other mechatronic and automotive systems that require similar levels of precision and robustness.

8 Future Work

The research presented in this dissertation has laid a substantial foundation for the development and control of modern Steer-by-Wire systems. However, there remain opportunities for further exploration and development: One area for potential future research involves improving the robustness of the system. Although this dissertation has proposed a novel robust control approach, exploring more advanced techniques may provide additional improvements. The integration of predictive control strategies and machine learning algorithms can enable real-time adaptation to changing driving conditions and system dynamics. Moreover, the development of adaptive control systems, which, for instance, learn from the driver's behavior and preferences, could offer a more personalized driving experience while maintaining safety and performance. Another opportunity is the integration of Steer-by-Wire systems with advanced driver assistance systems and functions for autonomous driving. Developing holistic control strategies that combine Steer-by-Wire with functions, such as lane-keeping assistance and collision avoidance, presents an opportunity for synergistic advances. This integration would require addressing challenges related to sensor fusion, interoperability and real-time data processing. Finally, extensive real-world testing and validation of Steer-by-Wire systems under various conditions should be pursued to fully understand their performance capabilities. Real-world testing across various weather conditions, terrains and vehicle types remains crucial for the final assessment of robustness and adaptability in practical applications.

9 Summary of Papers

The summaries of ***Paper I****,* ***Paper II****,* ***Paper III****,* ***Paper IV****,* ***Paper VI****,* ***Paper VII****,* ***Paper VIII****,* ***Paper IX****,* ***Paper X****,* ***Paper XI*** *and* ***Paper XII*** *are from the author's licentiate thesis [1].*

This chapter summarizes the content of the papers on which this dissertation is based upon and describes the author's contribution to each paper.

Paper I

Development and Analysis of a Detail Model for Steer-by-Wire Systems
This paper presents an innovative nonlinear detailed model of a Steer-by-Wire system. The detailed model represents all characteristics of a real Steer-by-Wire system. In the context of a dominance analysis of the detailed model, all dominant characteristics of a Steer-by-Wire system, including parameter dependencies, are identified. Through model reduction, a reduced model of the Steer-by-Wire system is then developed, which can be used for a subsequent robust control design. Furthermore, this paper compares the Steer-by-Wire system with a conventional electromechanical power steering and shows similarities as well as differences.

The author developed the detailed model of a Steer-by-Wire system, performed the analysis of the resulting model and identified the dominant characteristics of a Steer-by-Wire system as well as he developed optimal reduced models. In addition, he compared a Steer-by-Wire system with an electromechanical power steering. Moreover, the author wrote the paper.

Published in IEEE Access Journal in January 2023.

Paper II

Design of a Robust Optimal Multivariable Control for a Steer-by-Wire System

This paper presents a new control approach for modern Steer-by-Wire systems. The approach consists of a multivariable control for the driver's steering torque and the rack position simultaneously, using the requested torques of the downstream and upstream motors as control variables. The plant model used in this approach is a detailed model of a Steer-by-Wire system with nine degrees of freedom. For the control design, an optimal reduced model is derived. The reduced plant model is linearized, and it is augmented by linear models for the reference and disturbance environment of the Steer-by-Wire system and by a linearized model for the feeling generator, which computes the requested steering torque. For this augmented model, a multivariable linear optimal static state-space controller is designed. Hence, the entire environment of the real steering system is considered in the control design. Due to the multivariable approach and the augmented model containing all subsystems and dominant characteristics of the real system, the resulting control system shows excellent robustness characteristics.

The author developed the augmented model, performed the optimal multivariable control design and analyzed the resulting control system. Moreover, the author wrote the paper.

Published in SAE Technical Paper in March 2023, presented orally by the author in July 2023, Stuttgart, Germany.

Paper III

Direct Discrete Design of a Multivariable LQG Compensator with Combined Discretization Applied to a Steer-by-Wire System

This paper presents a direct discrete control design for modern Steer-by-Wire systems. The novel approach consists of a true multivariable control for both the driver's steering torque and the rack position simultaneously, using the requested torques of the downstream and upstream motors as control variables. For the control design, an optimal reduced plant model is used. It is derived from a detailed model of a Steer-by-Wire system with nine degrees of freedom. The reduced plant model is augmented by linear models for the reference and disturbance environment of the Steer-by-Wire system and discretized based on the characteristics of the input variables. For this augmented model, a direct discrete multivariable linear-quadratic-Gaussian compensator

is designed. The proposed control design considers the entire environment of the real steering system. The direct discrete approach restores the good characteristics of the continuous control and ensures that discretization does not have any adverse effects. Thus, the resulting discrete control system shows the same favorable dynamic characteristics as the continuous system.

The author developed a novel discretization method, performed the direct discrete control design and analyzed the resulting control system. Moreover, the author wrote the paper.

Published in Proceedings of Automotive meets Electronics, presented orally by the author in June 2023, Dortmund, Germany.

Paper IV

Design of a Model-Based Optimal Multivariable Control for the Individual Wheel Slip of a Two-Track Vehicle

This paper presents a model-based optimal multivariable control for the wheel slip, which allows specifying the wheel slip and thus the tire force individually for each wheel. The plant model consists of a multibody two-track model of a vehicle, a tire model, an air resistance model and a motor model. In addition, the contact forces of the individual wheels are calculated dynamically. The resulting nonlinear model is linearized and used for the design of a linear optimal static state-space controller with reference and disturbance feedforward. The contact point velocities at the wheels are defined as the controlled variables, since they are proportional to the wheel slip and thus to the driving forces within the operating range of the controller. Furthermore, the rates of change of the contact point velocities are also chosen as controlled variables to set the damping of the closed-loop system. The four drive torques of the wheels represent the control variables. Therefore, a true multivariable control is developed. In the first step of the analysis, the linearized closed-loop system is investigated regarding stability, robustness and its dynamic behavior. The control system shows a high bandwidth, well-damped dynamic behavior and a large phase margin. In the second step of the analysis, various simulations of realistic experiments, such as an accelerated cornering maneuver or the Fishhook road test, are performed with the nonlinear closed-loop system. The results of these experiments confirm the high robustness and good dynamic behavior of the control system in most cases. Moreover, the results demonstrate how the control considers the dynamic contact forces of the wheels to achieve the requested wheel slip at any time. Lastly, dominant transfer paths are identified based on the gain matrix of the state-space controller, showing

which input and state variables have a significant influence on the control variables.

The author developed the multibody model of the vehicle, an approach to approximate the contact forces and designed the optimal control. Moreover, the author elaborated the majority of the paper.

Published in SAE Technical Paper in March 2023, presented orally by Robert Rosenthal in July 2023, Stuttgart, Germany.

Paper V

Point Cloud based 3D Trafficability Analysis for Large-Volume and Heavy-Duty Transports

This paper presents an enhanced methodology for the three-dimensional trafficability analysis with collision detection of large-volume and heavy-duty transports. For this, the proposed approach uses high-resolution three-dimensional point clouds together with a detailed transport model. Furthermore, the methodology addresses the increasing complexity and challenges faced by stakeholders regarding transport planning. It emphasizes the need for detailed planning, especially for navigating through narrow passages along transportation routes. In addition, the approach is generalized and allows the automatic analysis of a variety of transport configurations, thus expanding its applicability to various scenarios.

The author developed the mathematical model of the transport and an approach for the efficient detection of collisions. Moreover, the author elaborated the majority of the paper.

Submitted to IET Intelligent Transport Systems in September 2024.

Paper VI

Methodical Data Collection for Light Electric Vehicles to Validate Simulation Models and Fit AI-based Driver Assistance Systems

This paper presents an approach to collect vehicle dynamics parameters for the validation of simulation models. For this purpose, a measurement system is developed to capture and monitor driving dynamic information of the device under test in real time. This data is used to fit pre-developed simulation models and DAS. To investigate the vehicle dynamics behavior in critical driving situations, an extensive test study is conducted. Therefore, different ordinary

driving situations in urban traffic scenarios are analyzed. Finally, the collected measured data is compared with the simulation results of a multibody model for a multi-lane cargo vehicle.

The author developed the simulation model, the measurement setup and the verification study. Additionally, he supervised the realization of the study. Moreover, the author wrote most parts of the paper.

Published in Proceedings of Kolloquium Future Mobility in June 2022, Ostfildern, Germany.

Paper VII

Integration of Vulnerable Road Users Behavior into a Virtual Test Environment for Highly Automated Mobility Systems

This paper describes an approach to integrate real human traffic behavior into the approval and testing process of highly automated vehicle systems. It provides a safe and valid way to test critical traffic scenarios between vehicles and pedestrians. Basically, two different methodologies for the metrological detection of human movements are analyzed and experimentally examined for their suitability for this application. Besides the general functionality, plausibility and real-time capability are further investigation criteria. The paper concludes with the integration of the proposed solution into a test bed for highly automated vehicle systems using a representative traffic scenario.

The author was involved in discussions, supported implementation and assisted in writing the paper.

Published in Proceedings of Kolloquium Future Mobility in June 2022, Ostfildern, Germany.

Paper VIII

Methodical Approach to Integrate Human Movement Diversity in Real-Time into a Virtual Test Field for Highly Automated Vehicle Systems

This paper measures, processes and integrates real human movement behavior into a virtual test environment for highly automated vehicle functionalities. The overall system consists of a georeferenced virtual city model and a vehicle dynamics model, including probabilistic sensor descriptions. By using motion capture hardware, real humanoid behavior is applied to a virtual human avatar

in the test environment. Through retargeting methods, the virtual avatar diversity is increased. To verify the biomechanical behavior of the virtual avatars, a qualitative study is performed, which is based on a representative movement sequence.

The author was involved in discussions, supported implementation and assisted in writing the paper.

Published in Journal of Transportation Technologies in July 2022.

Paper IX

Data Flow Management Requirements for Virtual Testing of Highly Automated Vehicles

This paper presents a virtual co-simulation approach for highly automated vehicle systems and uses it to demonstrate the data management requirements for a co-simulation platform such as AVL Model.CONNECT™. The basis for this is a real urban driving cycle for modern hybrid vehicles to investigate emissions, consumption and range as well as the effects of highly automated driving functions on these parameters.

The author was involved in discussions, supported conducting the study and assisted in writing the paper.

Published in Proceedings of AVL German Simulation Conference, presented orally by René Degen in September 2022, Regensburg, Germany.

Paper X

Stereoscopic Camera-Sensor Model for the Development of Highly Automated Driving Functions within a Virtual Test Environment

This paper documents the development of a sensor model for depth estimation of virtual three-dimensional scenarios. For this purpose, the geometric and algorithmic principles of stereoscopic camera systems are recreated in a virtual form. The model is implemented as a subroutine in the Epic Games Unreal Engine. Its architecture consists of several independent procedures, which enable a local depth estimation and a reconstruction of an entire three-dimensional scenery. In addition, a program for calibrating the model is presented.

The author was involved in discussions, assisted in writing the paper and supported implementation as well as evaluation.

Published in Journal of Transportation Technologies in January 2023.

Paper XI

Intelligent Analysis of Components with Regard to Significant Features for Subsequent Classification

This paper develops an intelligent method to analyze existing data appropriately and, at the same time, prepare it ideally for further applications, such as forecast models based on Artificial Intelligence. To achieve this, several steps need to be taken. Firstly, a suitable segmentation of the component is performed. The aim is to detect areas in a component where features and form elements are found. Other regions are ignored after the inspection by segmentation and voxelization. Subsequently, the voxelization of the component takes place, which results in the three-dimensional component or Computer-Aided-Design file being mathematically readable. This is done by rasterizing the component based on a previously selected resolution and other upcoming steps. Finally, the segmented and relevant areas are analyzed accordingly.

The author was involved in discussions and assisted in writing the paper.

Published in SAE Technical Paper, presented orally by Alexander Nüßgen in July 2023, Stuttgart, Germany.

Paper XII

Robustness and Sensitivity of Artificial Neural Networks for Mechatronic Product Development

This paper aims to evaluate the performance characteristics of different uncertainty analysis methods and assess their applicability in agile automotive development processes. By considering the specific requirements and constraints of each method, a decision tree is proposed to recommend suitable and situation-appropriate methods for performing uncertainty analyses in network prediction. The objective is to enhance data exchange between departments, mitigate disruptions and ensure informed decision-making throughout the development process.

The author was involved in discussions and assisted in writing the paper.

Published in Proceedings of Automotive meets Electronics, presented orally by Alexander Nüßgen in June 2023, Dortmund, Germany.

Paper XIII

Leveraging Robust Artificial Intelligence for Mechatronic Product Development – A Literature Review

This paper explores the existing literature regarding the application of AI as a comprehensive database, decision support system and modeling tool in mechatronic product development. It analyzes the benefits of AI in enabling domain linking, replacing human expert knowledge, improving prediction quality and enhancing intelligent control systems. For this purpose, a consideration of the V-model takes place, a standard in mechatronic product development. Along this, an initial assessment of the AI potential is shown and important categories of AI support are formed. This is followed by an examination of the literature with regard to these aspects. As a result, the integration of AI in mechatronic product development opens new possibilities and transforms the way innovative mechatronic systems are conceived, designed and deployed. However, the approaches are only taking place selectively, and a holistic view of the development processes and the potential for robust and context-sensitive AI along them is still needed.

The author was involved in discussions, assisted in writing the paper and supported evaluation.

Published in lnternational Journal of lntelligence Science in January 2024.

Paper XIV

Innovative Test Field Approach for Agricultural Applications

This paper discusses the growing need for near-operational complete vehicle tests in agricultural technology, driven by increasing automation levels. In order to validate novel assistance and automation functions that can interact with the tractor, implement and driver, more and more test kilometers are required. However, these additional kilometers consume additional time and are heavily influenced by weather conditions and seasonal availability of certain crops. Virtual test fields offer a solution by providing fully reproducible test scenarios, temporal independence and adjustable test parameters, making them more time and cost efficient. This paper explores the industry's needs and the state-of-the-art in highly realistic virtual test fields for agricultural applications. Based on this, a modular framework for implementation is presented, including the individual modules and their interfaces. Moreover, practical applica-

tion examples from the field of environment detection are provided, concluding with insights into future development perspectives and potential functional enhancements.

The author was involved in discussions, assisted in writing the paper and supported the identification of the modular framework.

Published in Proceedings of Fachtagung TestRig, presented orally by Martin de Fries in September 2024, Ostfildern, Germany.

Paper XV

Reinforcement Learning in Mechatronic Systems: A Case Study on DC Motor Control

This paper explores the integration of artificial intelligence in mechatronic product development, focusing on the use of reinforcement learning as a control strategy. It examines the application of reinforcement learning during crucial stages of the product development lifecycle, particularly between system architecture, system integration and verification. A reinforcement learning-based controller is created and evaluated against a traditional proportional-integral controller in dynamic and fault-prone environments. The results demonstrate the adaptability, stability, and optimization capabilities of the reinforcement learning approach, particularly in addressing dynamic disturbances and ensuring robust performance. Moreover, the findings emphasize the potential of AI-driven methodologies to transform the design of intelligent mechatronic systems. Future research will include incorporating domain-specific knowledge into the reinforcement learning process and validating this approach in real-world settings.

The author was involved in discussions, assisted in writing the paper and advised on modeling and control.

Published in Circuits and Systems in January 2025.

10 Svensk Sammanfattning

Denna avhandling presenterar modellbaserad design och styrning av avancerade fordonsystem, med primärt fokus på moderna Steer-by-Wire-system, som är kritiska för implementeringen av högautomatiserade och autonoma fordon. Jämfört med konventionella elektromekaniska styrsystem kännetecknas Steer-by-Wire-system av att de inte har en mekanisk koppling mellan fordonets ratt och framhjul. Även om denna frånvaro har fördelar som designflexibilitet och integration av ny teknik, medför den också betydande utmaningar för att säkerställa styrningens robusthet och fordonssäkerhet. Denna avhandling behandlar dessa utmaningar genom att först presentera den teoretiska bakgrunden för mekatroniska system och deras utvecklingsprocesser. Den beskriver strukturen hos mekatroniska system, introducerar modellbaserade designmetoder och diskuterar implementeringen av virtuell testning. Därefter beskrivs utvecklingen av en detaljerad modell för Steer-by-Wire-system, som tar hänsyn till alla relevanta frihetsgrader och icke-linjära egenskaper som kan uppstå i ett verkligt Steer-by-Wire-system. Denna modelleringsmetod utgör grunden för den följande styrdesignen.

En ny multivariabel styrmetod utvecklas sedan för att förbättra robustheten och prestandan hos Steer-by-Wire-system. Nuvarande styrmetoder utför vanligtvis separata single-input single-output designer, vilket kan påverka robustheten hos det övergripande styrsystemet. Denna avhandling introducerar en optimal tillstånd-rymdregulator, som visar överlägsen systemstabilitet och prestanda jämfört med konventionella styrmetoder som PID- eller kaskadregulatorer. Den nya styrningen analyseras därefter både i tids- och frekvensdomänen inom en utökad simuleringsmiljö för att verifiera dess robusthet mot obeaktat beteende, parameterosäkerheter och varierande körförhållanden.

Förutom virtuell testning inkluderar avhandlingen praktiska experiment med en prototyp för att validera den föreslagna styrmetoden i verkliga miljöer. Denna praktiska validering är avgörande eftersom den överbygger gapet mellan teoretisk design och funktionell realisering, och visar på fördelarna med den modellbaserade designmetoden genom att minska behovet av omfattande fysiska tester och därmed optimera utvecklingstid och resurser.

Utöver utvecklingen av Steer-by-Wire-system omfattar avhandlingen också ytterligare tillämpningar inom fordonsteknik, såsom förarassistanssystem, sensorevalueringar och perceptionssystem. Den utvecklade virtuella simuleringsmiljön underlättar inte bara analysen av dessa komponenter utan stöder också avancerade studier av fordonsbeteende och trafikinteraktionsmodellering. Exempel på denna utökade tillämpning inkluderar utvecklingen av modeller för stora och tunga transporter samt lastcyklar, som båda visar mångsidigheten och robustheten hos de tillämpade modellbaserade designmetoderna.

Sammanfattningsvis bidrar forskningsresultaten till områdena mekatronik och fordonsingenjörskonst genom att främja möjligheterna för autonoma körfunktioner genom robusta styrsystem, virtuella testmetoder och agila utvecklingsstrategier. Dessutom främjar denna avhandling inte bara förståelsen och implementeringen av Steer-by-Wire-system, utan kan också tjäna som en grund för framtida forskning och utveckling inom mekatroniska system som kräver precis styrning och tillförlitlighet. De presenterade metoderna och insikterna bidrar till utvecklingen av nästa generations fordonsystem, med betoning på modellbaserad design och robusta styrmetoder som avgörande för att uppnå hög prestanda och säkerhetsstandarder i moderna fordonsapplikationer. Framtida forskning kan utvidga dessa strategier till att omfatta ett bredare spektrum av fordonsinnovationer, och kontinuerligt förbättra precisionen, effektiviteten och hållbarheten hos fordonsystem.

11 Deutsche Zusammenfassung

Diese Arbeit befasst sich mit dem modellbasierten Entwurf und der Regelung moderner Fahrzeugsysteme, wobei der Schwerpunkt auf Steer-by-Wire-Systeme gelegt wird, die für den Einsatz hochautomatisierter und autonomer Fahrzeuge erforderlich sind. Im Vergleich zu konventionellen elektromechanischen Servolenkungen zeichnen sich Steer-by-Wire-Systeme durch das Fehlen einer mechanischen Verbindung zwischen dem Lenkrad und den Vorderrädern eines Fahrzeugs aus. Dieser Umstand hat zwar Vorteile, wie z.B. Flexibilität bei der Konstruktion und die Integration neuer Komponenten, stellt aber auch eine große Herausforderung für die Robustheit der Lenkungsregelung, die Fahrzeugsicherheit sowie die Rückmeldung eines gewünschten Lenkgefühls dar. Die vorliegende Dissertation befasst sich mit diesen Herausforderungen, indem sie zunächst den theoretischen Hintergrund mechatronischer Systeme und ihrer Entwicklungsprozesse darstellt. Sie beschreibt die Struktur mechatronischer Systeme, stellt modellbasierte Entwurfsmethoden vor und erörtert die Implementierung virtueller Testverfahren. Anschließend wird die Entwicklung eines detaillierten Modells für Steer-by-Wire-Systeme beschrieben, das alle relevanten Freiheitsgrade und nichtlinearen Eigenschaften berücksichtigt, die in einem realen Steer-by-Wire-System auftreten können. Diese detaillierte Modellbildung bildet die Grundlage für den folgenden Regelungsentwurf.

Hierbei wird ein neuartiger Ansatz zur Mehrgrößenregelung entwickelt, um die Robustheit und Performanz von Steer-by-Wire-Systemen zu verbessern. Derzeitige Regelungsansätze führen in der Regel separate SISO-Entwürfe durch, die bei anschließender Kopplung die Robustheit des gesamten Regelungssystems beeinträchtigen können. In dieser Dissertation wird ein optimaler Zustandsraumregler eingeführt, der im Vergleich zu herkömmlichen Regelungsansätzen eine bessere Stabilität und Güte aufweist. Die daraus resultierende neuartige Regelung wird anschließend sowohl im Zeit- als auch im Frequenzbereich in einer erweiterten Simulationsumgebung analysiert, um ihre Robustheit gegenüber nicht berücksichtigtem Streckenverhalten, Parameterschwankungen und variierenden Umgebungsbedingungen zu verifizieren.

Zusätzlich zu den virtuellen Tests umfasst die Dissertation praktische Experimente mit einem Prototyp, um den vorgeschlagenen Regelungsansatz in

seiner realen Betriebsumgebung zu validieren. Diese praktische Validierung ist unerlässlich, da sie die Lücke zwischen dem theoretischen Entwurf und der funktionalen Realisierung schließt und so die Vorteile des modellbasierten Entwurfs hervorhebt, indem sie die Notwendigkeit umfangreicher physischer Tests reduziert und somit die Entwicklungszeit und -ressourcen optimiert.

Neben der Entwicklung von Steer-by-Wire-Systemen werden in der Dissertation die Methoden auch auf weitere Anwendungen in der Fahrzeugtechnik, wie z.B. Fahrerassistenzsysteme, Sensorauswertungen und Perzeptionssysteme, ausgeweitet. Die entwickelte Simulationsumgebung erleichtert nicht nur die Analyse dieser Komponenten, sondern unterstützt auch fortgeschrittene Untersuchungen im Bereich des Fahrzeugverhaltens und der Modellierung der Verkehrsinteraktion. Beispiele für diese erweiterte Anwendung sind die Entwicklung von Modellen für Großraum- und Schwertransporte sowie Lastenfahrräder, die beide die Vielseitigkeit und Robustheit der angewandten modellbasierten Entwurfsmethodik demonstrieren.

Zusammenfassend tragen die Forschungsergebnisse zu den Bereichen Mechatronik und Fahrzeugtechnik bei, indem sie die Voraussetzungen für autonome Fahrfunktionen durch robuste Regelungssysteme, virtuelle Testmethoden und agile Entwicklungsstrategien schaffen. Darüber hinaus fördert diese Dissertation nicht nur das Verständnis und die Implementierung von Steer-by-Wire-Systemen, sondern kann auch als Grundlage für zukünftige Forschung und Entwicklung mechatronischer Systeme dienen, die eine präzise Regelung bei gleichzeitig hoher Robustheit erfordern. Die vorgestellten Methoden und Erkenntnisse helfen bei der Entwicklung von Fahrzeugsystemen der nächsten Generation und betonen dabei den modellbasierten Entwurf sowie robuste Regelungsansätze als entscheidend für das Erreichen hoher Performanz- und Sicherheitsstandards. Zukünftige Forschungsarbeiten könnten diese Ansätze auf ein breiteres Spektrum von Innovationen im Automobilbereich ausweiten, um die Präzision, Effizienz und Nachhaltigkeit von Fahrzeugsystemen kontinuierlich zu verbessern.

12 Acknowledgement

First and foremost, I would like to express my gratitude to my supervisor Margot Ruschitzka for giving me the opportunity to conduct my PhD studies and for her invaluable mentorship throughout this journey. Her support has been of great help to my academic development. I am also deeply thankful to my supervisor Karin Thomas. Her support and insights regarding the specific aspects of research at the Division of Electricity at Uppsala University were particularly valuable. My sincere thanks also go to my supervisor Hermann Henrichfreise, who took time for enriching technical discussions. His innovative ideas significantly contributed to the successful outcomes of this dissertation.

Furthermore, I would like to thank Georg Engelmann and Markus Pütz, who, as deans, gave me the opportunity to be employed at TH Köln during my PhD studies. I also thank Mats Leijon for granting me the chance to start my PhD studies in cooperation with Uppsala University. Moreover, my appreciation also goes to DMecS Development of Mechatronic Systems GmbH & Co. KG for sharing their practical expertise and their support during my research.

Additionally, I am grateful to my colleagues at both TH Köln and Uppsala University. Their collaborative spirit and support have been a source of strength and inspiration. Finally, I would like to express my thankfulness to my family, friends and above all, my wife, for their unwavering support and encouragement. Their belief in me has been a constant source of motivation.

References

[1] Irmer, M., “Model-Based Design and Virtual Testing of Steer-by-Wire Systems,” licentiate thesis, Uppsala University, Sweden, 2023.

[2] ZF Friedrichshafen AG, “Networked Steering With “Steer-by-Wire”,” https://www.zf.com/mobile/en/technologies/vehicle_motion_control/stories/sbw.html, accessed 27.02.2025.

[3] HELLA GmbH & Co. KGaA, “HELLA develops series production-ready key components for all-electric steer-by-wire systems,” Press release, Lippstadt, Germany, 2022.

[4] Robert Bosch GmbH, “Steer-by-wire – Steering technology of the future,” https://www.bosch-mobility.com/en/solutions/steering/steer-by-wire, accessed 27.02.2025.

[5] Isermann, R., “Mechatronic Systems – Fundamentals,” Springer London, England, 2005.

[6] VDIVDE-Gesellschaft Mess- und Automatisierungstechnik, “Development of mechatronic and cyber-physical systems (VDI/VDE 2206),” VDI/VDE, Germany, 2021.

[7] The MathWorks, Inc., “Model-Based Design,” https://de.mathworks.com/solutions/model-based-design.html, accessed 27.02.2025.

[8] Tränkle, F., “Modellbasierte Entwicklung Mechatronischer Systeme,” de Gruyter, Germany, 2021.

[9] Deutsches Institut für Normung e. V., “Straßenfahrzeuge – Fahrzeugdynamik und Fahrverhalten – Begriffe (ISO 8855:2011),” Beuth, Germany, 2011.

[10] Betzler, J., “Fahrwerktechnik: Grundlagen,” Vogel, Germany, 2005.

[11] Stoll, H., “Fahrwerktechnik: Lenkanlagen und Hilfskraftlenkungen,” Vogel, Germany, 1992.

[12] Robert Bosch GmbH, “Kraftfahrtechnisches Taschenbuch,” Springer Vieweg, Germany, 2024.

[13] Cheon, D., Lee, C., Oh, S., Nam, K., “Description of Steering Feel in Steer-by-Wire System Using Series Elastic Actuator,” Proc. 2019 IEEE Vehicle Power and Propulsion Conference, October 2019, Hanoi, Vietnam.

[14] Grüner, S., Werner, T., Käpernick, B., “Objectification of steering feel and application in the context of virtual steering feel tuning,” Proc. 8th International Munich Chassis Symposium, June 2017, Munich, Germany.

[15] Balachandran, A., Gerdes, J. C., “Designing Steering Feel for Steer-by-Wire Vehicles Using Objective Measures,” IEEE/ASME Transactions on Mechatronics, Vol. 20, No. 1, pp. 373-383, February 2015.

[16] Dannöhl, C., “Entwicklung eines Algorithmus zur Servokraftregelung einer elektromechanischen Lenkung,” Ph.D. dissertation, Technical University of Munich, Germany, 2010.

[17] Pfeffer, P., Harrer, M., “Lenkungshandbuch – Lenksysteme, Lenkgefühl, Fahrdynamik von Kraftfahrzeugen,” Springer Vieweg, Germany, 2013.

[18] Lunkeit, D., “Ein Beitrag zur Optimierung des Rückmelde- und Rückstellverhaltens elektromechanischer Servolenkungen,” Ph.D. dissertation, University of Duisburg-Essen, Germany, 2014.
[19] Buschardt, B., “Synthetische Lenkmomente,” Ph.D. dissertation, Technische Universität Berlin, Germany, 2003.
[20] von Groll, M., “Modifizierung von Nutz- und Störinformationen am Lenkrad durch elektromechanische Lenksysteme,” Ph.D. dissertation, University of Duisburg-Essen, Germany, 2006.
[21] Rill, G., “Simulation von Kraftfahrzeugen,” Vieweg & Teubner, Germany, 2007.
[22] Henrichfreise, H., Jusseit, J., Niessen, H., “Optimale Regelung einer elektromechanischen Servolenkung,” Proc. Fachtagung Mechatronik, May 2003, Fulda, Germany.
[23] Graßmann, O., Henrichfreise, H., Niessen, H., Hammel, K. v., “Variable Lenkunterstützung für eine elektromechanische Servolenkung,” Proc. 23. Tagung Elektronik im Kraftfahrzeug, June 2003, Essen, Germany.
[24] Irmer, M., Henrichfreise, H., “Robust generation of a steering feel for electric power steering systems,” Proc. Digital-Fachtagung Mechatronik, March 2021, Darmstadt, Germany.
[25] Niessen, H., Henrichfreise, H., “Vehicle steering system for controlling a steering or steering lock angle for at least one wheel of a vehicle,” International Patent No. WO 02/076806 A1, World Intellectual Property Organization, 2002.
[26] Mortazavizadeh, S. A., Ghaderi, A., Ebrahimi, M., Hajian, M., “Recent developments in the vehicle steer-by-wire system,” IEEE Transactions on Transportation Electrification, Vol. 6, No. 3, pp. 1226–1235, September 2020.
[27] Isermann, R., Schwarz, R., Stolzl, S., “Fault-tolerant drive-by-wire systems,” IEEE Control Systems Magazine, Vol. 22, No. 5, pp. 64–81, October 2002.
[28] Bröcker, M., “New Control Algorithms for Steering Feel Improvements of an Electric Powered Steering System with Belt Drive,” Vehicle System Dynamics, No. 44, pp. 759-769, January 2006.
[29] Chen, X., Chen, X., “Control-Oriented Model for Electric Power Steering System,” Proc. SAE 2006 World Congress & Exhibition, April 2006, Detroit, USA.
[30] El-Shaer, A. H., Sugita, S., Tomizuka, M., “Robust Fixed-Structure Controller Design of Electric Power Steering Systems,” Proc. 2009 American Control Conference, July 2009, St. Louis, USA.
[31] Fahami, S. M. H., Zamzuri, H., Mazlan, S. A., Zakaria, M. A., “Modeling and simulation of vehicle steer by wire system,” Proc. 2012 IEEE Symposium on Humanities, Science and Engineering Research, June 2012, Kuala Lumpur, Malaysia.
[32] Bertoluzzo, M., Buja, G., Menis, R., Sulligoi, G., “An approach to steer-by-wire system design,” Proc. 2005 IEEE International Conference on Industrial Technology, December 2005, Hong Kong, China.
[33] Badawy, A., Zuraski, J., Bolourchi, F., Chandy, A., “Modeling and analysis of an electric power steering system,” Proc. Steering and Suspension Technology Symposium 1999, March 1999, Warrendale, USA.
[34] dSPACE GmbH, “ASM Vehicle Dynamics,” Automotive Simulation Models, Paderborn, Germany, 2023.

[35] Chitu, C., Lackner, J., Horn, M., Srikanth Pullagura, P., Waser, H., Kohlböck, M., "Controller design for an electric power steering system based on LQR techniques," COMPEL – The international journal for computation and mathematics in electrical and electronic engineering, No. 32.3, pp. 763-775, May 2013.
[36] Milbaier, P., Grüner, S., Heger, M., Gaedke, A., "Evaluation of the robustness of an EPS control System in an early stage of the product development life cycle," Proc. 8th International Munich Chassis Symposium, June 2017, Munich, Germany.
[37] Bao, C., Feng, J., Wu, J., Liu, S., Xu, G., Xu, H., "Model predictive control of steering torque in shared driving of autonomous vehicles," Science Progress, No. 103.3, September 2020.
[38] Ewald, V., "Regelung redundant aktuierter Steer-by-Wire Systeme," Ph.D. dissertation, Technical University of Darmstadt, Germany, 2021.
[39] Gonschorek, R, Bertram, T, "Robust Two-Degrees of Freedom Linear Quadratic Gaussian Position Control for the Front Axle Actuator of a Steer-by-Wire System," Engineering Research, Vol. 87, No. 2, February 2023.
[40] Irmer, M., Haßenberg, M., Briese, H., Henrichfreise, H., "Robust Control of an Electric Power Steering with unconsidered Modes and Parameter Uncertainties," Proc. 10th International Munich Chassis Symposium, June 2019, Munich, Germany.
[41] Irmer, M., Haßenberg, M., Briese, H., Henrichfreise, H., "Mechatronic system design for EPS systems with residual modes and variable, nonlinear plant behavior," Proc. 20. Internationales Stuttgarter Symposium, March 2020, Stuttgart, Germany.
[42] Irmer, M., Henrichfreise, H., "Design of a robust LQG Compensator for an Electric Power Steering," Proc. 21st IFAC World Congress, July 2020, Berlin, Germany.
[43] Wittler, G., Haßenberg, M., Briese, H., Schubert, T., Henrichfreise, H., "Systematic model-based vibration analysis of a controlled electric power steering system," Proc. 8th International Munich Chassis Symposium, June 2017, Munich, Germany.
[44] Schiehlen, W., Eberhard, P., "Applied Dynamics," Springer Cham, Switzerland, 2014.
[45] Pfeiffer, F., "Mechanical System Dynamics," Springer Berlin, Germany, 2008.
[46] Parkus, H., "Mechanik der festen Körper," Springer Vienna, Austria, 2005.
[47] Gonschorek, R., Bertram, T., "Linear-quadratic-Gaussian position control of the hand wheel actuator for a steer-by-wire steering system," Proc. Digital-Fachtagung Mechatronik, March 2021, Darmstadt, Germany.
[48] Schölzel, M., Scholand, M., Kleiner, C., Wesche, M., Ein Waldt, A., Nehls, O., "Basic Safety Guidelines for Steer-by-Wire for a New DIN Standard," Proc. 13th International Munich Chassis Symposium, July 2022, Munich, Germany.
[49] Farshizadeh, E., "Regelungskonzept für eine elektrohydraulische Bremsanlage mit adaptivem Bremsgefühl," Ph.D. dissertation, Otto-von-Guericke University Magdeburg, Germany, 2017.
[50] Föllinger, O., "Regelungstechnik – Einführung in die Methoden und ihre Anwendung," VDE Verlag, Germany, 2016.
[51] Lunze, J., "Regelungstechnik 2 – Mehrgrößensysteme, Digitale Regelung," Springer Vieweg, Germany, 2020.
[52] Hrycej, T., "Robuste Regelung – Ein Leitfaden für sicherheitskritische Anwendungen," Springer Vieweg, Germany, 2018.

[53] Friedland, B., “Control System Design – An Introduction to State-Space Methods,” Dover Publications, USA, 2005.
[54] Unbehauen, H., “Regelungstechnik II – Zustandsregelungen, digitale und nichtlineare Regelsysteme,” Springer Vieweg, Germany, 2007.
[55] Franklin, G. F., Powell, D. J., Workman, M. L., “Digital Control of Dynamic Systems,” Prentice Hall, USA, 1997.
[56] Henrichfreise, H., “Prototyping of a LQG Compensator for a Compliant Positioning System with Friction,” TransMechatronik, Vol. 23, No. 1, 1997.
[57] Irmer, M., Henrichfreise, H., “Design of a Simulation Environment for Testing the Control of Electric Power Steering Systems,” Proc. 21. Internationales Stuttgarter Symposium, March 2021, Stuttgart, Germany.
[58] Schramm, D., Hiller, M., Bardini, R., “Modellbildung und Simulation der Dynamik von Kraftfahrzeugen,” Springer Berlin, Germany, 2018.
[59] Shadmehr, R., Wise, S. P., “Computational Neurobiology of Reaching and pointing: A Foundation for Motor Learning,” MIT Press, USA, 2005.
[60] Haas, A., Menze, G., Sieberg, P., Schramm, D., “Evaluation of Feedback Behavior of Steering Systems on a mHiL-Steering-Test-Bench,” Proc. 23. Internationales Stuttgarter Symposium, July 2023, Stuttgart, Germany.
[61] Isermann, R., Münchhof, M., “Identification of Dynamic Systems – An Introduction with Applications,” Springer Berlin, Germany, 2011.
[62] Pick, A. J., Cole, D. J., “Dynamic properties of a driver’s arms holding a steering wheel,” Journal of Automobile Engineering, Vol. 221, No. 12, pp. 1475–1486, December 2007.
[63] Schenk, L., Chugh, T., Bruzelius, F., Shyrokau, B., “Musculoskeletal Driver Model for the Steering Feedback Controller,” Vehicles, Vol. 3, No. 1, pp. 111–126, February 2021.
[64] Hemmersbach, M., Briese, H., Haßenberg, M., Irmer, M., Henrichfreise, H., “Application of a Detailed Model of a Steering System in Highly Dynamic HiL Tests of EPS Motors,” Proc. 21. Internationales Stuttgarter Symposium, March 2021, Stuttgart, Germany.
[65] National Highway Traffic Safety Administration, “Laboratory Test Procedure for Dynamic Rollover – The Fishhook Maneuver Test Procedure,” U.S. Department of Transportation, USA, 2015.
ISO 3888-1:2018, “Passenger cars – Test track for a severe lane-change manoeuvre – Part 1: Double lane-change,” International Organization for Standardization, Switzerland, 2018.

Acta Universitatis Upsaliensis

Digital Comprehensive Summaries of Uppsala Dissertations from the Faculty of Science and Technology 2516

Editor: The Dean of the Faculty of Science and Technology

A doctoral dissertation from the Faculty of Science and Technology, Uppsala University, is usually a summary of a number of papers. A few copies of the complete dissertation are kept at major Swedish research libraries, while the summary alone is distributed internationally through the series Digital Comprehensive Summaries of Uppsala Dissertations from the Faculty of Science and Technology. (Prior to January, 2005, the series was published under the title "Comprehensive Summaries of Uppsala Dissertations from the Faculty of Science and Technology".)

Distribution: publications.uu.se
urn:nbn:se:uu:diva-552408

ACTA UNIVERSITATIS
UPSALIENSIS
2025